Reactions of U^+ with H_2, D_2, and HD Studied by Guided Ion Beam Tandem Mass Spectrometry and Theory

Wen-Jing Zhang,[1] Maria Demireva[1,†] JungSoo Kim,[1] Wibe. A. de Jong,[2] and P. B. Armentrout[1,]*

[1]Department of Chemistry, University of Utah, Salt Lake City, Utah 84112-0850, USA

[2]Lawrence Berkeley National Laboratory, One Cyclotron Road, Berkeley, California 94720, USA

ABSTRACT

The kinetic energy dependent reactions of the atomic actinide uranium cation (U^+) with H_2, D_2, and HD were examined by guided ion beam tandem mass spectrometry. An average 0 K bond dissociation energy of $D_0(U^+-H) = 2.48 \pm 0.06$ eV is obtained by analysis of the endothermic product ion cross sections. Quantum chemistry calculations were performed for comparison with experimental thermochemistry, including high-level CASSCF-CASPT2-RASSI calculations of the spin-orbit corrections. CCSD(T) and the CASSCF levels show excellent agreement with experiment, whereas, B3LYP and PBE0 slightly overestimate and the M06 approach badly underestimates the bond energy for UH^+. Theory was also used to investigate the electronic structures of the reaction intermediates and potential energy surfaces. The experimental product branching ratio for reaction of U^+ with HD indicates that these reactions occur primarily via a direct reaction mechanism, despite the presence of a deep-well for UH_2^+ formation according to theory. The reactivity and hydride bond energy for U^+ are compared with those for transition metal, lanthanide, and actinide cations, and periodic trends are discussed. These comparisons suggest that the *5f* electrons on uranium are largely core and uninvolved in the reactive chemistry.

[†]Present address: Sandia National Laboratories, Livermore, CA 94551

Corresponding Author: *P. B. Armentrout, 315 S 1400 E Rm 2020, Salt Lake City, UT 84112-0850. armentrout@chem.utah.edu; Phone: +1 (801) 581 – 7885

Introduction

The thermochemistry and reactivity of actinide (An) containing species are of significant interest because of their inherent importance in the nuclear fuel cycle: recovery of fissile materials from seawater, reprocessing of nuclear fuel, safe storage of nuclear waste, the mitigation of groundwater contamination using advanced separations technologies,[1] and because *f*-orbitals make them fundamentally intriguing. Despite such interest, the radioactivity of most actinides (except Th and U) has limited their study to dedicated laboratories. Theoretical studies of actinides are attractive because safety concerns are mitigated; however, the actinides require comprehensive treatments of both relativistic and electron correlation effects. Thus, the accurate description of the experimental properties of actinides by *ab initio* methods is difficult and can require extensive multireference methods because of the large number of low-lying molecular electronic states resulting from occupation of low-energy *5f* and *6d* shells. To date, gas-phase experimental work has dealt primarily with reactions of early actinide elements Th-Cm including hydrocarbon activation reactions[2-10] and oxidation.[11-19] The challenge of heavy-element studies results in several examples of discrepancies (real or apparent) between experimental and theoretical thermochemistry in the literature.[20-23] Some errors result from experimental work,[21] whereas others seem to be related to the theoretical methods.[20,22-23] Some of these discrepancies may be avoided in the future if high quality benchmark experimental data were available for comparison to results from high levels of theory.

Experimentally, uranium metal and H_2 react to form UH_3, which can release H_2 at high temperature.[24] In matrix isolation experiments using an argon matrix, UH_n (n = 1 − 4) and U_2H_m (m = 2 and 4) have been observed and their vibrational frequencies reported.[25] Addition of more H_2 leads to a $UH_4(H_2)_6$ structure, which computations show is a central tetrahedral UH_4 molecule with six dihydrogen molecules bonding parallel to each edge of the tetrahedron.[26] Other calculations have indicated that UH_6 spontaneously decomposes by loss of H_2.[27] In the gas-phase, among the simplest reaction systems that can be studied in detail both experimentally and theoretically is the reaction of atomic ions with H_2 and its isotopologues. Previously, Moreland,

Rokop, and Stevens[28] observed the formation of UH$^+$ (UD$^+$) in the reactions of atomic uranium cations with H_2, H_2O, and H_2S (and their perdeuterated variants), and estimated that the bond dissociation energy (BDE) of UD$^+$ was 3.3 ± 0.5 eV. Armentrout, Hodges, and Beauchamp examined the kinetic energy dependence of the endothermic reactions of U$^+$ with D_2 and CD_4 using an ion beam apparatus.[2] From analysis of the thresholds for production of UD$^+$, they assigned the experimental BDE of UH$^+$ as 2.9 ± 0.2 eV. Marçalo and Gibson used ion cyclotron resonance mass spectrometry (ICR-MS) to study the reactions of An^{2+} (including U^{2+}) with alkanes and alkenes.[9] They observed that UH$^+$ + $C_3H_7^+$ was formed in reaction with propane, which leads to a lower limit for D_0(U$^+$-H) of ≥ 0.97 ± 0.2 eV presuming IE(U$^+$) = 10.6 eV,[29] or of D_0(U$^+$-H) ≥ -0.13 ± 0.2 eV if IE(U$^+$) = 11.7 ± 0.3 eV is used.[19] Using B3LYP/SDD-VDZ-MWB/6-311+G(p) and PW91/ZORA theoretical approaches, Di Santo et al. reported UH$^+$ BDEs of 2.35 and 2.94 eV, respectively,[30] where the latter value is in good agreement with the experimental values. However, this same work calculated the BDE of ThH$^+$ as 2.98 and 3.49 eV, respectively, i.e., considerably stronger than D_0(UH$^+$) at both levels of theory. Both of these theoretical values are much higher than an experimental value for D_0(ThH$^+$) of 2.45 ± 0.07 eV recently measured by examination of the reactions of Th$^+$ with CH_4[23] and H_2, HD, and D_2,[31] using a guided ion beam tandem mass spectrometer (GIBMS). In the latter work, BDEs of other actinide hydride cations (AnH$^+$) were estimated on the basis of D_0(Th$^+$-H) and the promotion energy (E_P) associated with excitation from the ground level to a state having the appropriate electronic configuration for forming a strong single covalent bond (ignoring the energy associated with spin decoupling the bonding electron from other unpaired electrons on the metal).[19] Because the promotion energies of Th$^+$ and U$^+$ are similar (0.0 and 0.04 eV), this analysis suggested that the UH$^+$ BDE (estimated to be 2.41 ± 0.07 eV) should be similar to that of ThH$^+$. Indeed, the analogous prediction works well for ThF$^+$ and UF$^+$ BDEs (also single covalent bonds with extensive ionic character), which are measured as 6.63 ± 0.10 and 6.57 ± 0.10 eV, respectively.[29,31-34]

Here, we report the absolute cross sections as a function of kinetic energy for the reactions of atomic uranium cations with H_2, D_2, and HD as measured using a GIBMS. Analysis of the kinetic energy dependence of these cross sections permits direct determination of $D_0(U^+$-H). Theoretical calculations of UH^+ and UH_2^+ were also performed to assign electronic states, compare to the experimental bond energy, and to explore possible reaction mechanisms. As our group has previously examined the analogous reactions with atomic metal cations of first-row,[35-42] second-row,[40,42-44] and third-row[45-49] transition metals, several lanthanides,[40,50-51] and the actinide Th^+,[31] the present study allows an evaluation of the periodic trends in this simplest of all exchange reactions.

Experimental and Theoretical Methods

Instrument. The GIBMS used in these experiments and the general experimental procedures have been described in detail previously.[52-53] Briefly, uranium cation precursor ions were created using a direct current discharge/flow tube source (DC/FT),[54] described in more detail below. After exiting the source, U cations were focused and $^{238}U^+$ ions were mass selected using a magnetic momentum analyzer. These ions were decelerated to a well-defined kinetic energy and injected into a radio frequency (rf) octopole ion guide that trapped the ions radially.[55-56] The octopole passed through a static pressure reaction cell containing the neutral reaction partner (H_2, HD, or D_2) at sufficiently low pressures (0.1 - 0.4 mTorr) that single collision conditions prevailed. All cross sections were measured at several pressures to ensure that rigorous single-collision conditions were used in the data analysis. Product and remaining precursor ions drifted to the end of the octopole, where they were extracted, separated with a quadrupole mass filter, and detected using a secondary electron scintillation (Daly) detector.[57] Reaction cross sections at each relative kinetic energy were converted from product ion intensities relative to reactant ion intensities after correcting for background ion intensities measured when the neutral gas was no longer directed into the gas cell, as described previously.[52] Uncertainties in these absolute product ion cross sections are estimated to be ±20%, with relative

cross sections accurate to about ±5%. Laboratory (lab) ion energies were converted to the center-of-mass (CM) frame using the relationship $E_{CM} = E_{lab} \times m/(m + M)$ where m and M are the masses of the neutral and ionic reactants, respectively. Cross sections are known to be broadened by the kinetic energy distribution of the reactant ions and the thermal (300 K) motion of the neutral reactant.[58-59] The absolute zero of energy and the full width at half-maximum (fwhm) of the ion beam were determined by using the octopole guide as a retarding potential analyzer.[52] Typical fwhms of the energy distribution for these experiments were 0.3 – 0.5 eV (lab) and the uncertainty in the energy scale was ±0.1 eV (lab). All energies reported below are in the CM frame.

Ion source. The DC/FT source has been described in detail previously.[54] Briefly, a uranium metal sample (^{238}U, 99.79% abundance, New Brunswick Laboratory) was held at about -1.0 kV. The resultant electric field ionized Ar gas that flowed over the cathode in a 9:1 He/Ar mixture. The ionized Ar collided with the cathode and U^+ ions were sputtered and swept into the flow tube by the He/Ar flow at typical pressures of 0.5–0.7 Torr. In the flow tube, ions were thermalized by $\sim 10^5$ collisions with carrier gases. Previous experiments utilizing the DC/FT source with transition metal cations have indicated that the internal energies of the atomic cations generated can be characterized by effective temperatures of 300 – 1100 K.[44,60-64] An equilibrium population analysis at 300 K indicates that 76.2% of U^+ is in its ground level ($^4I_{9/2}$,$5f^37s^2$) and 22.8% of U^+ is in its first excited level ($^6L_{11/2}$,$5f^36d7s$) at 289.0 cm^{-1} (0.036 eV).[29,65] At 1100 K, these populations change to 42.7% and 35.1% with additional contributions of 12.9%, 6.1%, and 2.5% in excited levels ($^6K_{9/2}$,$5f^36d7s$), ($^6L_{13/2}$,$5f^36d7s$), and ($^6K_{11/2}$,$5f^36d7s$) at 914.8, 1749.1, and 2294.7 cm^{-1} (0.113, 0.217, and 0.285 eV), respectively. Conservatively, we estimate the internal temperature to be 700 ± 400 K, where U^+ has an average electronic energy of $E_{el} = 240 \pm 172$ cm^{-1} (0.03 ± 0.02 eV).

Data analysis. The kinetic energy dependence of endothermic reactions was modeled using eq 1,[66-69]

$$\sigma(E) = \sigma_0 \Sigma\, g_i\, (E + E_{el} + E_i - E_0)^n/E \qquad (1)$$

where σ_0 is an energy independent scaling factor, E is the relative kinetic energy of the reactants, E_{el} is defined above, E_i is the internal energy of the reactant neutral (vibrational and rotational for H_2, D_2, and HD) having populations g_i ($\Sigma g_i = 1$), n is an adjustable parameter, and E_0 is the 0 K reaction threshold. Before comparison to the data, eq 1 was convoluted over the kinetic energy distributions of the reactants.[52] The σ_0, n, and E_0 parameters were then optimized using a nonlinear least-squares method to best reproduce the experimental cross section. Uncertainties in E_0 were calculated from the threshold values from several independent data sets (minimum of five for each system) and combined with the absolute uncertainties in the kinetic energy scale (<0.001 eV) and electronic energies of reactant ions (0.02 eV). The E_0 thresholds were used to determine the bond dissociation energy (BDE), $D_0(U^+-H)$, using eq 2 and its isotopic analogues.

$$D_0(U^+-H) = D_0(H-H) - E_0 \qquad (2)$$

Equation 2 assumes that there are no barriers in excess of the endothermicity of the reaction.[70] No experimental or theoretical evidence was found to suggest that such a barrier is present.

Above the neutral reactant BDE, product ions can have enough internal energy to dissociate. To account for this effect, eq 1 is multiplied by the probability for dissociation of the products, P_D, using a simple model detailed elsewhere.[71] P_D is controlled by two parameters: E_D, the energy where dissociation begins, and p, similar to n but limited to integral values, that controls how rapidly the cross section declines. The p and E_D parameters were optimized to best reproduce the high-energy cross sections without affecting the threshold energy determinations.

Theoretical calculations. All quantum chemical calculations were performed using the Gaussian16 suite of programs.[72] For most calculations, a correlation consistent polarized core valence, including core-valence correlation corrections, quadruple-ζ basis set, cc-pwCVQZ-MDF (20s17p12d11f7g4h1i)/[9s9p8d8f7g4h1i]) developed by Peterson[73] that utilizes the Stuttgart/Koeln fully relativistic small core (60 electron) effective core potential (ECP60MDF pseudopotential),[74] was used for U^+ along with the aug-cc-pVQZ basis set[75] for H. For calculating BDEs, several additional basis sets were used. For U^+, these include the Stuttgart Dresden basis set (SDD-VDZ-MWB) with its accompanying small core quasirelativistic ECP (MWB) available

on the EMSL basis set exchange,[76-77] a segmented basis set (Seg. SDD-VQZ-MWB) that utilizes the MWB ECP,[78] atomic natural orbital basis sets designed for use with the MWB (ANO-VQZ-MWB)[78] and MDF (ANO-VQZ-MDF)[74] ECPs, and correlation consistent cc-pVTZ-MDF, cc-pVQZ-MDF, and cc-pwCVTZ-MDF (which include core−valence correlation) basis sets[73] with the MDF ECP. Pople 6-311+G(3pd), cc-pVTZ, cc-pVQZ, aug-cc-pVTZ, and aug-cc-pVQZ basis sets[75] were used for H. Additionally, BDEs were calculated utilizing the all-electron variants of cc-pVXZ (cc-pVXZ-DK3) and cc-pwCVXZ (cc-pwCVXZ-DK3) basis sets[73] (where X = T or Q) and B3LYP/cc-pwCVQZ-MDF/aug-cc-pVQZ optimized structures. These latter calculations were performed using the second order Douglas−Kroll−Hess Hamiltonian (DK2).[79-84] Of note is that the all-electron basis sets were formulated for use with a third order Douglas−Kroll−Hess Hamiltonian (DK3), but the DK3 calculations cannot be performed presently in Gaussian16. Use of DK2 may lead to errors, which are anticipated to be small.[85] Extrapolation to the complete basis set limit (CBS) was performed using the Karton−Martin method,[73,86] eq 3, proposed for the HF energies with the TZ (X = 3) and QZ (X = 4) energies.

$$E_X = E_{CBS} + A(X + 1)e^{-6.57\sqrt{X}} \tag{3}$$

For CCSD(T) calculations, eq 4 was used to extrapolate the correlation energy.[73,87-88]

$$E_X = E_{CBS} + B(X + \tfrac{1}{2})^{-4} \tag{4}$$

Calculations also utilized density functional theory (DFT) methods, B3LYP,[89-90] M06,[91] and PBE0 (PBE1PBE).[92-93] Of these functionals, B3LYP and M06 have been shown to perform well for actinide–oxygen bond energies and for ionization energies of actinide oxides and their cations.[94] PBE0 has previously yielded similar geometrical structures as B3LYP in previous Th$^+$ studies.[23,31] Additionally, CCSD(T),[95-98] a coupled cluster method that mixes single and double excitations with perturbative triple excitations, was used for single point calculations using the B3LYP optimized structures. For CCSD(T) electron correlation calculations, the $5s$ and $5p$ electrons were usually frozen. All calculations were open-shell and unrestricted, and all energies discussed below were corrected by the zero-point energy using the frequencies generated for their respective optimized structure after scaling by 0.989.[31,99] No significant spin contamination

was observed in these calculations for any species studied. Natural bond orbital (NBO) analyses[100-101] of states were also conducted to determine the orbital occupations of most states.

Spin-orbit energy correction estimates were obtained using complete active space SCF (CASSCF)[102] followed by second order multiconfigurational perturbation theory (CASPT2)[103] to estimate dynamical correlation effects and subsequent restricted active space state interaction (RASSI)[104] to compute the spin-orbit eigenstates. This approach is similar the one used by Bross and Peterson, Antonov and Heaven, and Dolg and Cao for estimating the role of spin-orbit on the spectra of UF^+, UCl^+, and the spectra and BDE of UH.[85,105-106] The relativistic Atomic Natural Orbital (ANO-RCC-VXZP with X = D, T, Q) basis sets available in OpenMolcas were used. The relativistic DK2 Hamiltonian was used to compute the scalar relativistic and spin-orbit coupling effects. Following Bross and Peterson, state-averaged CASSCF and CASPT2 were used to generate ^5I, ^5L, and ^3I states for UH^+ and U^{2+} and ^6L and ^4I states for U^+ in each irrep of the C_2 point group (yielding symmetries a and b), using an active space consisting of the *5f*, *6d*, and *7s* orbitals for U^+. For UH^+, the same active space was used and doubly occupied H^- orbital was included in the inactive space. In the subsequent CASPT2 calculations, the U(*6s*), U(*6p*), and the doubly-occupied H(*1s*) orbitals were also correlated. The default OpenMolcas IPEA shift of 0.25 and imaginary shift of 0.1 were used in the CASPT2 calculations, with the multi-state optimization turned off. All generated states were included in the RASSI calculations to generate the spin-free and spin-orbit states. The ground state was used for the calculation of the BDE.

Experimental Results

$U^+ + H_2$ and D_2. The reactions of U^+ with H_2 and D_2 yield products according to reactions 5 and 6.

$$U^+ + H_2 \quad \rightarrow \quad UH^+ + H \tag{5}$$

$$U^+ + D_2 \quad \rightarrow \quad UD^+ + D \tag{6}$$

The kinetic energy dependent cross section for reaction 5 can be found in Figure 1 with the analogous deuterium cross section in Figure 2. Reactions 5 and 6 have apparent thresholds near

1.5 eV with the cross sections peaking near $D_0(H_2)$ = 4.478 eV and $D_0(D_2)$ = 4.556 eV.[107-108] Above these energies, the cross sections decrease because the internal energies of the UH^+ and UD^+ products increase, leading to dissociation to U^+ + H (D), which has an onset equal to $D_0(H_2)$ or $D_0(D_2)$. The magnitude at the maximum UH^+ and UD^+ cross sections are similar at 5.12 and 5.15 $Å^2$), respectively, well within the estimated absolute cross section uncertainty (±20%).

Figure 2 also includes a reproduction of the data from the previous ion beam experiment of Armentrout, Hodges, and Beauchamp (AHB).[2] It can be seen that the absolute cross section measurements obtained here agree with these previous measurements in the threshold region up to about 3 eV, where the previous data plateaus rather than continuing to increase. Because this instrument did not incorporate an rf octopole ion guide, its ability to measure accurate cross sections over a wide range of energies was compromised. In particular, complete collection of product ions at higher collision energies was unlikely because of increasingly large transverse energies. Differences in the cross sections in the threshold region can be attributed to differences in the source of the uranium cations and the collision cell temperature (400 K versus the 300 K used here). AHB generated their ions using a surface ionization source operated at an estimated temperature of 2300 K, such that many excited electronic states are occupied. The average electronic energy at this temperature is 0.19 eV with states up to 0.69 eV having populations exceeding 1%. The effects of this are evaluated further below.

U^+ + HD. Reaction of U^+ with HD yields products according to reactions 7 and 8,

$$U^+ + HD \quad \rightarrow \quad UH^+ + D \tag{7}$$

$$\rightarrow \quad UD^+ + H \tag{8}$$
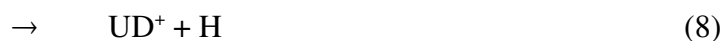
as shown in Figure 3. Reactions 7 and 8 have similar apparent thresholds as reactions 5 and 6 and their cross sections peak near $D_0(HD)$ = 4.514 eV.[107-108] At energies somewhat above the apparent thresholds, UH^+ is found to be the dominant product by about a 2:1 ratio. The magnitude of the total cross section at its peak (6.2 $Å^2$) is 1.2 times the magnitude of the peak cross sections for reactions 5 and 6, within the 20% absolute experimental uncertainty.

Thermochemical Results. The fitting parameters of eq 1 augmented by the model for

dissociation (P_D) that were used to model the cross sections of reactions $5 - 8$ can be found in Table 1. The models including the effects of dissociation are shown in Figures $1 - 3$ and can be seen to reproduce the data throughout the entire energy range examined. Because the model of eq 1 explicitly accounts for the internal energy of all reactants, the E_0 values reported in Table 1 are thresholds at 0 K. It can be seen that the thresholds for all four reactions are similar. Given literature values for the BDEs of H_2, D_2, and HD (noted above), the thresholds measured for reactions $5 - 8$ can be converted using eq 2 (or its isotopic analogues) to $D_0(U^+-H)$, as listed in Table 1 after correcting the values obtained for UD^+ products for a zero-point energy difference of 0.029 eV (calculated using a vibrational frequency for UH^+ of 1593 cm^{-1}, see below). The weighted average of these four measurements is $D_0(U^+-H) = 2.48 \pm 0.06$ eV, where the uncertainty is one standard deviation.

The present result is consistent with the lower limits for $D_0(U^+-H)$ obtained in the ICR study of the reactions of U^{2+} with alkanes and alkenes,[9] and in good agreement with the BDE of 2.41 ± 0.07 eV estimated on the basis of $D_0(Th^+-H)$ and $E_P(U^+) = 0.04$ eV (see above).[29,31,65] Our present $D_0(U^+-H)$ value is much lower than the value of 2.9 ± 0.2 eV,[2] measured by AHB in early ion beam studies of the reactions of U^+ with D_2 and CD_4. These data were analyzed using a linear function that accounted for the thermal motion of the D_2 gas, but not the internal energies of either reactant. Indeed, if the present data are reanalyzed assuming a D_2 gas temperature of 400 K and an electronic distribution for U^+ at 2300 K, one obtains a threshold that differs from the present analysis by 0.5 eV, such that this amount of the discrepancy is immediately attributable to the different experimental conditions. This correction would change the 1.7 ± 0.1 eV threshold for reaction 6 reported by AHB to a 0 K value of 2.2 ± 0.1 eV, within experimental uncertainty of the threshold determined here, 2.08 ± 0.08 eV. Differences in the two results should also result from the use of a linear function to interpret the more limited data set (approximately eight data points) in the older experiment.

Reaction Mechanism. The product branching ratio in the endothermic reaction $M^+ + HD$ is sensitive to the reaction mechanism, as shown in previous work with transition metals.[43-44,109]

Three possible reaction mechanisms were established for strictly diabatic behavior where the M^+ electronic configuration remains static through the course of the reaction. (1) If M^+ has an electronic configuration with empty s and $d\sigma$ orbitals, such as a d^n configuration where n < 5, the reaction proceeds efficiently by an insertion mechanism. These processes exhibit statistical behavior associated with a long-lived HMH^+ intermediate and have branching ratios (σ_{MH}/σ_{Tot}) near 0.5. (2) If M^+ has an electronic configuration with occupied valence s or $d\sigma$ orbitals and is low-spin, such as for d^n where n > 5 or low-spin coupled $d^{n-1}s^1$ configurations, the reaction proceeds efficiently via a direct mechanism. These processes are consistent with a short-lived interaction between M^+ + HD such that conservation of angular momentum favors MH^+ over MD^+ by factors of 2−4, leading to σ_{MH}/σ_{Tot} between 0.66 and 0.80. (3) If M^+ has an electronic configuration with occupied valence s or $d\sigma$ orbitals and has the highest possible spin state, such as a high-spin coupled $d^{n-1}s^1$ configuration, the reaction proceeds inefficiently by an impulsive mechanism. Here, the metal cation interacts strong with only one of the atoms (H or D), such that the effective kinetic energy is different for each interaction. Such processes favor MD^+ + H by a large factor and thresholds shifted from thermodynamic values by large amounts.

The cross section branching ratio, $[\sigma_{UH}/\sigma_{Tot}]$, obtained in the present work lies near 0.7 from threshold until 4.5 eV, where it gradually increases to 0.86 at 7.0 eV. The latter increase has been explained previously,[35,109-110] and results from the fact that the heavier D atom can take away a larger amount of translational energy than the lighter H atom. The branching ratio below 4.5 eV indicates that the uranium cation system exhibits behavior in class 2, a direct reaction.

Ignoring the *5f* orbitals (which may be reasonable as previous studies indicate minimal participation of *5f* orbitals in the bonding of the diatomics UF, UF^+, UO and UO^+),[85] the expected diabatic reactivity of the ground level of U^+ ($^4I_{9/2}$, $5f^37s^2$), which should have an experimental population of 76 − 43%, is inefficient and impulsive (class 3 above) because the fully occupied *7s* orbital should interact repulsively with H_2. In contrast, the experimentally occupied $^6L_{11/2}$ ($5f^36d7s$), 23 − 35% population, and $^6K_{9/2}$ ($5f^36d7s$), 1 − 13% population, levels should evolve along surfaces that are more attractive and should react via direct processes (class 2 behavior).

Some indication of whether the ground level is reactive or not can be obtained from a comparison of the absolute cross sections for reactions 5 – 8, peak magnitudes of 5 – 6 Å^2, with those for other metal cations in the analogous reactions. The other actinide we have studied, Th$^+$, exhibited peak magnitudes of 3 – 4 Å^2,[31] while the lanthanide, Gd$^+$ (^{10}D, *4f^{7}5d6s*), was 1.0 – 1.3 Å^2.[50] Group 3 transition metal cations exhibited peak magnitudes of about 0.7, 1.1, 1.5, and 0.8 Å^2 for Sc$^+$ (^{3}D, *3d4s*), Y$^+$ (mainly ^{3}D, *4d5s*), La$^+$ (mainly ^{3}F, *5d^2*), and Lu$^+$ (^{1}S, *6s^2*).[40] Thus, the relative magnitudes of the cross sections measured here suggest that there is no component of the experimental ion population that is unreactive. As a consequence, the experimental result indicates that the surface evolving from the ^{4}I$_{9/2}$ level probably undergoes an avoided crossing with a Ω = 9/2 surface evolving from the ^{6}K$_{9/2}$ (*5f^{3}6d7s*) level, only 0.113 eV above the ground level.[29,65] Crossings with other surfaces (e.g., ^{6}L$_{11/2}$ at 0.036 eV)[29,65] might also occur but only if the Ω quantum number need not be conserved during reaction. These conclusions can be tested further by examination of the theoretical results.

Theoretical Results

Energy Levels of U$^+$. One way to gauge the accuracy of a theoretical method is to compare predicted low-lying states of the atomic metal cation to those observed experimentally, as previously done for U$^+$ by Di Santo et al.[30] Here, we compare low-lying states calculated using the cc-pwCVQZ-MDF basis set and several levels of theory to experimental excitation energies in Table 2, with additional levels included in Table S1 of the Supporting Information. The experimental energies listed are weighted averages over all spin−orbit levels of each state,[29,65] which is problematic for several states of U$^+$, as experimental levels for ^{6}L$_{21/2}$, ^{6}K$_{19/2}$, ^{6}M$_{21/2}$, and ^{6}M$_{23/2}$ have not been identified spectroscopically. These energy levels were estimated by extrapolation from the other J levels in the same term.

All levels of theory correctly predict a ^{4}I ground state (although a sextet state that is mainly *5f^{4}7s* character mixed with *5f^{3}6d7s* lies 0.03 eV lower at PBE0 levels of theory, see also Table S1). Furthermore, B3LYP, M06, and CCSD(T) with the cc-pwCVQZ-MDF basis set

correctly predict the ordering of ^{4}I ($5f^37s^2$), ^{6}I ($5f^47s$), and ^{6}M ($5f^36d^2$) states, Table 2. When the electron configuration is $5f^36d7s$, ^{6}H, ^{6}K, and ^{6}L states result and have an experimental energy range between 0.42 – 0.50 eV. B3LYP, M06, PBE0, and CCSD(T) levels of theory locate multiple $5f^36d7s$ states, and these were assigned to match the experimental order. Notably, freezing the $5s$ and $5p$ electrons leads to better results for the CCSD(T) calculations, an effect that has been discussed by Bross and Peterson, who find that these orbitals stabilize the ^{4}I state.[105]

Spin-Orbit Energy Corrections. Unless explicit spin-orbit (SO) calculations are conducted, theoretical energies correspond to a value that has been averaged over all SO states whereas experimental 0 K energies correspond to the lowest levels of the species. Therefore, valid comparisons between experimental and theoretical values must include SO effects, which are large for U$^+$. For the BDE of UH$^+$, SO corrections require that the U$^+$ + H asymptote be lowered by the empirical difference between the U$^+$ (^{4}I$_{9/2}$) ground level and the ground state energy averaged over all SO levels, a difference of 0.849 eV. In addition, the BDE should be corrected for the SO splitting of UH$^+$, which is unknown. In the absence of better information, we could assume that the calculated SO splitting value of UH$^+$ is the same as that for ground state UF$^+$ (^{5}I). Here, a value of 0.568 eV is determined from the average energy of the Ω = 4, 5, 6, 7, 8 levels of the ^{5}I state equally weighted by their two-fold degeneracy as calculated by Bross and Peterson at 0, 1061, 3784, 7101, and 10978 cm^{-1}, respectively.[105] According to this assumption, theoretically calculated BDEs for UH$^+$ should be decreased by 0.849 – 0.568 = 0.281 eV. Alternatively, because these states are very atomic like, one could weight them by 2Ω + 1, in which case the SO correction is 0.675 eV for UH$^+$, leading to a decrease in the BDE of 0.174 eV. Fortunately, these assumptions are not needed in the present work as explicit calculations of the SO corrections for UH$^+$ are provided in the following section.

Energy Corrections from CASSCF-CASPT2-RASSI Calculations. The SO was calculated for the UH$^+$ and U$^+$ atom with the relativistic DK2 Hamiltonian using the CASSCF-CASPT2-RASSI level of theory. The calculated bond lengths and binding energies, plus the spin-orbit corrections for U$^+$, UH$^+$, and the BDE are listed in Table 3. Note that some additional

calculations were performed with the relativistic DK3 and X2C Hamiltonian,[111] which yielded similar results. As can be seen in the last column of Table 3, the SO correction of 0.852 eV obtained with the DK2-CASSCF-CASPT2-RASSI approach for U^+ is in good agreement with the experimental result of 0.849 eV. For the molecule, the $\Omega = 4, 5, 6, 7, 8$ levels in UH^+ show a similar behavior compared to those of Bross and Peterson for UF^+.[105] Overall, the results in Table 3 show that the UH^+ BDEs should be decreased by 0.074 eV.

The magnitude of the calculated SO correction for the UH^+ BDE is attributed to the difference in atomic spin-orbit corrections for U^+ and U^{2+}. For a DKH calculation using an all-electron basis set, Cao, Moritz, and Dolg calculated a SO correction for the ground state (mainly ^4I) of neutral UH of 0.08 and 0.12 eV depending on the method used.[112] Balasubramanian calculated an effect of 0.09 eV for UH_2.[113] In a subsequent paper, Dolg and Cao improved their results and found a larger SO correction for UH of 0.2 eV.[106] Their SO correction of 0.2 eV for UH is closely matches the change in SO corrections based on the experimental atomic energy levels of U (1.041 eV) and U^+ (0.849 eV). For U^{2+}, the largest J-values have not been resolved experimentally for the ^5I ($5f^37s$) and ^5L ($5f^36d$) levels relevant for the UH^+ molecular structure. Using CASSCF-CASPT2-RASSI calculations for U^{2+}, the J=8 level of the ^5I ($5f^37s$) is estimated to be ~12,300 cm^{-1}. Combining this with the known experimental atomic levels for J=5-7, properly weighted by atomic degeneracies, the SO effect on $^5I_4$ ($5f^37s$) is estimated to be 0.771 eV. Using this estimate, the net effect on the BDE based on atomic SO corrections for U^+ and U^{2+} (0.849 and 0.771 eV, respectively) is estimated to be 0.078 eV, which is very similar to the result obtained for the UH^+ molecule.

The energy of the SO interaction can also be given by $E^{SO} = A \Lambda M_S$, where A is the SO splitting constant for uranium and Λ and M_S are the orbital and spin angular momentum quantum numbers for a particular $\Omega = \Lambda + M_S$ level.[114] Given E^{SO} ($^5I_4$) = -0.779 eV where $\Lambda = 6$ and $M_S = -2$, this formula provides A = 0.065 eV. (Alternatively, if E^{SO} ($^5I_4$) from the UF^+ calculations, -0.568 eV, is used, then A = 0.047 eV.) Presuming this value of A can be utilized for other states

of UH$^+$, which should be a good approximation presuming the occupied orbitals have similar character, SO corrections can be evaluated for any other state.

Electronic States of UH$^+$. CASSCF calculations correlating six electrons in the U(*5f*, *6d*, *7s*) and H(*1s*) orbitals indicate that the ground state is largely a single reference state near the equilibrium geometry. Hence, the present calculations should provide a reasonable description of UH$^+$. The present results for calculations of ground and excited states of UH$^+$ are listed in Table 4. As noted above, CCSD(T) and B3LYP results provide the most accurate atomic excitation energies and therefore our theoretical results for UH$^+$ will focus on these results (with others provided in the supporting information Table S2). Here, the ground state of UH$^+$ has a $^5\Phi$ ($1\sigma^2 2\sigma[\pi^2\varphi]$) valence electron configuration, where orbitals in square brackets indicate largely nonbonding *5f* orbitals of U. The 1σ bonding molecular orbital (MO) couples the H *1s*-orbital with a mainly *6d*σ orbital of U$^+$ and the nonbonding 2σ MO comprises mostly the U$^+$ *7s*-orbital with some *6d*-character. The next five excited states located all have quintet spin and differ only in the *5f* orbital populations. Consequently, these states lie below 0.15 eV in excitation energy and have similar bond lengths (1.98 ± 0.01 Å) and vibrational frequencies (~1590 cm^{-1}). These results agree with previous calculations where a $^5\Lambda$ ground state with a bond length of 2.07 Å was found by the SCF treatment of Krauss and Stevens.[115] Di Santo et al. located a $^5\Delta$ ground state in B3LYP/SDD-VDZ-MWB/6-311+G(p) calculations.[116] Balasubramanian[113] found a $^5\Lambda$ ground state using MP2 and CCSD(T) levels, with a ^{3}I state lying 0.23 and 0.27 eV higher, respectively, whereas his B3LYP calculations predicted a ^{3}I ground state, 0.09 eV lower in energy than the quintet state. Further, bond lengths calculated in the present work are consistent with the previous MP2 results of 1.97 Å for the $^5\Lambda$ state, however, a shorter bond length of 1.863 Å was reported for the ^{3}I state.[113] Slightly higher vibrational frequencies than current work were reported previously by Balasubramanian, 1652 and 1817 cm^{-1}, respectively,[113] whereas Krauss and Stevens got 1515 cm^{-1} for their $^5\Lambda$ ground state.[115]

We also located several states of UH$^+$ with triplet and singlet spin that result from spin pairing the *5f* electrons of the quintet states while retaining the $1\sigma^2 2\sigma$ valence electrons. Again,

this leads to similar bond lengths and vibrational frequencies, Table 4. The triplet states lie between 0.23 and 0.84 eV higher than the ground state, in agreement with the MP2 and CCSD(T) calculations of Balasubramanian.[113] We also located singlet states lying 0.88 – 1.15 eV above the ground state and a $^3\Delta$ state having a $1\sigma^2 1\delta$ valence occupation in which the 1δ orbital is a pure $6d$ on U. This change increases the energy of this state appreciably, increases the bond length, and decreases the vibrational frequency compared to the other states, Table 4.

After including SO corrections using A = 0.065 eV, the order of the different states changes, with the most significant change being the ground state switching to a ^{5}I ($1\sigma^2 2\sigma[\pi\delta\varphi]$) electron configuration at both B3LYP and CCSD(T) levels. (The same ground state is obtained using A = 0.047 eV.) This result is consistent with previous work showing that ^{5}I is the ground state for UF$^+$ (which agrees with the assumption made above).[105] It can also be seen that the excitation energy of the triplet and singlet states increases, with the lowest of these lying 0.623 and 1.653 eV above the ^{5}I state, Table 4. For the $^3\Delta$ ($1\sigma^2 1\delta[\sigma\delta^2/\sigma\varphi^2]$) state, there is also an additional SO correction associated with the 1δ electron. For this, we utilize the ζ_d parameter calculated for the $5f^3 6d^2$ configuration by Meftah et al. of 1410 cm^{-1} (0.175 eV).[117]

Importantly, all states having a $1\sigma^2 2\sigma[5f^3]$ configuration diabatically correlate with the low-lying excited U$^+$ (^{6}L$_{11/2}$, $5f^3 6d7s$) + H (^{2}S) and U$^+$ (^{6}K$_{9/2}$, $5f^3 6d7s$) + H (^{2}S) asymptotes, lying only 0.036 and 0.113 eV above ground level U$^+$(^{4}I$_{9/2}$, $5f^3 7s^2$) + H (^{2}S). The excited $^3\Delta$ ($1\sigma^2 1\delta[\sigma\delta^2/\sigma\varphi^2]$) state of UH$^+$ correlates with the excited U$^+$ (^{6}M$_{13/2}$, $5f^3 6d^2$) + H (^{2}S) asymptote, 0.569 eV above U$^+$(^{4}I$_{9/2}$) + H. None of the low-lying UH$^+$ states diabatically correlate with the U$^+$(^{4}I$_{9/2}$, $5f^3 7s^2$) + H (^{2}S) ground level.

Potential Energy Surfaces for UH$^+$. Table 5 lists the theoretical BDEs of ground level UH$^+$ for various levels of theory and basis set combinations (with Supporting Information Table S3 listing additional theoretical results). The SO correction determined above from UF$^+$ indicates that the theoretical BDEs should be reduced by 0.281 eV, whereas the CASSCF-CASPT2-RASSI calculations indicate a reduction of only 0.074 eV. The ground state is ^{5}I after accounting for SO energy for all levels of theory and either SO correction. The CCSD(T) BDEs at the

complete basis set (CBS) limit using a SO correction of -0.074 eV (2.36 – 2.45 eV) are in excellent agreement with the experimental value of 2.48 ± 0.06 eV, whereas the SO correction taken from UF^+ leads to much lower BDEs (2.15 – 2.24 eV). This result makes it clear that the SO correction calculated here is reliable, and that the UH^+ and UF^+ systems are not directly analogous, as discussed above. The SO corrected BDE obtained from the CASSCF-CASPT2-RASSI calculations of 2.34 eV (see Table 3) is in close agreement with the CCSD(T) results. BDEs predicted by B3LYP (2.52 – 2.55 eV) lie somewhat above the experimental value, whereas the PBE0 results are even higher (by another 0.15 eV). M06 level calculations grossly underestimate the experimental BDE (both with and without SO corrections) by at least 0.5 eV (see Table S3).

In the previous theoretical work of Balasubramanian,[113] no BDEs for UH^+ were reported, whereas Krauss and Stevens[115] report D_e = 2.1 eV with ω_e = 1515 cm^{-1}, such that D_0 = 2.0 eV, substantially weaker than the present theoretical values. Di Santo et al. report a UH^+ BDE of 2.35 eV calculated at their B3LYP/SDD level and a much larger 2.94 eV for PW91/ZORA calculations;[30] however, the latter level of theory has been found to overestimate BDE values in other systems.[23] Further, in the case of U^+, PW91/ZORA calculations incorrectly predict the ground state of U^+, whereas the B3LYP/SDD approach was successful in this regard.[30]

Electronic States of UH_2^+. To explore the mechanism of the reaction of U^+ with H_2, we have also examined computationally the UH_2^+ intermediates that might be formed. Representative ground and excited states calculated for UH_2^+ are listed in Table 6 with a full listing provided in Table S4 of the Supporting Information. This compilation is undoubtedly not comprehensive as different occupations of the *5f* orbitals lead to multiple states having the same symmetry. In the following discussion, CCSD(T) energies will be used but B3LYP values are generally within 0.3 eV.

The ground state (GS) of UH_2^+ is a dihydride species in a $^4A_1$ state with a $(1a_1)^2(1b_2)^2[1a_2^{1}1b_1^{1}2b_2^{1}]$ electron configuration where the three unpaired electrons are found in U^+ (*5f^3*) orbitals, again designated in square brackets. The $1a_1$ bonding MO is a *6d$_{z^2}$7s* hybridized

orbital on U interacting with the H ($1s$) orbitals, and the $1b_2$ MO is a bonding interaction of the $6d_{yz}$ and the H ($1s$) orbitals (where the z-axis is defined as the C_2 symmetry axis and the molecule lies in the yz-plane). It can be noted that this intermediate lies 0.538 eV below the $U^+(^4I) + H_2$ asymptote and has a HU^+-H BDE calculated as 2.57 eV (no SO corrections), similar to the 2.51 eV BDE for U^+-H calculated at the same level of theory (again no SO correction). There are two other $^4A_1$ states close in energy (0.065 and 0.142 eV above the GS, Table S4). These $^4A_1$ states have the same bonding orbitals as the $^4A_1$ GS with variations in the occupied $5f$ MOs. These variations also lead to series of three $^4A_2$, two $^4B_1$, and three $^4B_2$ states having similar bond lengths (1.991 – 2.000 Å) and bond angles (94° – 102°), and excitation energies of 0.004 – 0.369 eV, Table S4. Other excited $^4A_1$ and $^4B_1$ states of the dihydrides lying ~1.76 eV above the GS were found in which one $5f$ electron is moved into a $6d_{xy}$ ($2a_2$) orbital. This leads to shorter bond lengths (near 1.93 Å) but similar bond angles. There is also a series of low-lying doublet states (three $^2B_2$, one $^2A_2$, and one $^2B_1$) that have the same bonding MO population, $(1a_1)^2(1b_2)^2$, but the three $5f$ electrons are low-spin coupled. Thus, the bond angles and bond lengths are similar to those found for the quartet states, but they have higher energies (0.72 – 0.83 eV), consistent with Hund's rules.

We also located a series of linear HUH^+ molecules having both quartet and sextet spin. The valence MOs of these states are $1\sigma^2$ and $2\sigma^1$, which correspond to a bonding combination of the $6d\sigma$ and $H_2(\sigma_g)$ orbitals and the $7s$ orbital, respectively. They also occupy the $5f\sigma$ orbital, which also has some bonding character as it mixes with the empty $H_2(\sigma_u*)$. Both high-spin sextet and low-spin quartet species can be formed by altering the coupling between the singly occupied 2σ and the four $5f$ electrons. Two of the quartet states doubly occupy the $5f\sigma$ orbital and therefore have bond lengths of 1.97 and 1.96 Å and lie 1.75 and 1.93 eV above the $^4A_1$ ground state. All other states singly occupy the $5f\sigma$ orbital such that they have longer U^+-H bonds, 2.11 – 2.16 Å, and lie at higher energies, 2.49 – 3.0 eV above the $^4A_1$ ground state. (Other higher lying states were also located but are not included in Table 6.) In some cases, these linear molecules prefer to distort by bending, leading to molecules with large angles, ∠HUH between 137° –

167°, and longer U$^+$–H bond lengths, 2.12 – 2.17 Å. These states also lie high in energy, 2.57 – 3.04 eV.

In addition to these large angle species, minima are also observed at small ∠HUH angles, Table 6, corresponding to U$^+$(H$_2$) association complexes. Many of these intermediates are characterized by ∠HUH near 20° with r(H–H) of approximately 0.8 Å, similar to r(H–H) = 0.742 Å calculated for free H$_2$. Additionally, these species have r(U$^+$–H) = 2.21 – 2.41 Å, significantly longer than the bond lengths of the large angle HUH species. Excitation energies of these adducts are 0.73 – 1.45 eV. Here the valence orbitals are generally $(1a_1)^2(1b_2)^1(3a_1)^1$ where the 1a$_1$ is mainly the H$_2$(σ_g) orbital with some $6d_{z2}$ character, the 1b$_2$ remains the $6d_{yz}$ coupling with the H$_2$(σ_u), and 3a$_1$ is mainly the $7s$ orbital on U with some $6d_{z2}$ hybridization. Sextet states (two $^6A_1$, one $^6A_2$, two $^6B_1$, three $^6B_2$) having $(1a_1)^2(1b_2)^1(3a_1)^1[5f\ ^3]$ configurations have bond angles of 19° – 20°, UH bond lengths of 2.31 – 2.36 Å, and lie 0.73 – 1.06 eV above the GS. Doublet (two $^2A_2$, one $^2B_1$) and quartet (one $^4A_1$, two $^4A_2$, three $^4B_1$, two $^4B_2$) states having the same electronic configuration have bond angles of 19° – 22°, bond lengths of 2.21 – 2.41 Å, and excitation energies of 1.07 – 1.45 eV. Higher lying states, one sextet ($^6A_1$) having a $(1a_1)^2(1b_2)^1(3b_1)^1[5f\ ^3]$ configuration and one sextet ($^6A_1$) and one quartet ($^4A_2$) having $(1a_1)^2(1b_2)^1(2a_2)^1[5f\ ^3]$ configurations, were also found. We also located four quartet states with even smaller HUH bond angles (near 11°) and longer UH bond lengths (near 4 Å), which lie only ~0.5 eV above the $^4A_1$ ground state. These states have $(1a_1)^2(3a_1)^2[5f^3]$ configurations where neither the 1a$_1$ nor the 3a$_1$ MOs have any appreciable $6d_{z2}$ character, consistent with only ion-induced dipole interactions with the U$^+$ (^{4}I, $5f^37s^2$) ground state. Other variants with similar bond angles lie at higher energy as well and include both doublet and quartet states.

Potential Energy Surfaces for UH$_2$$^+$. In order to explore the potential energy surfaces of reaction 5, we performed relaxed potential energy surface scans along the ∠HUH coordinate using the optimized UH$_2$$^+$ structures as starting geometries. As noted above, DFT methods yielded similar results regardless of the basis set used for UH$^+$ and this parallels results obtained in our studies of Th$^+$ + H$_2$ and Th$^+$ + CH$_4$ reactions.[23,31] Consequently, to avoid excessive

computational cost, PES scans were performed using the B3LYP/Seg. SDD-VQZ-MWB/6-311+G(3dp) level of theory. The results for C_{2v} symmetry orientations separated into those having the same C_s symmetry (the symmetry of the experimental collisions) are presented in Figures 5 (with A′ symmetry) and S1 (with A″ symmetry). As discussed below, these surfaces differ primarily in the particular *5f* orbitals occupied, hence the character of both A′ and A″ surfaces are very similar. Notably, neither zero-point energies nor SO effects are included in this diagram. Finally, a comparison of these surfaces with those of Balasubramanian for the neutral reaction of U + H$_2$ shows very parallel results,[113] lending confidence to the present work.

As U$^+$ in its various electronic states approaches H$_2$, attractive wells leading to the U$^+$(H$_2$) adducts discussed above are formed. Correlation between these surfaces and the asymptotic energies of the U$^+$ + H$_2$ reactants is imperfect, probably because the calculations do not encompass the multireference character of these surfaces. As ground state U$^+$ (^{4}I) and H$_2$ approach perpendicularly (side-on), the two H$_2$(σ_g) electrons combine with the two *7s* electrons on U$^+$ to form doubly occupied 1a$_1$ bonding and 3a$_1$ antibonding orbitals. Not surprisingly, the *7s^2* configuration of U$^+$(^{4}I) leads to a very shallow well and relatively repulsive surface. These wells correspond to the adducts identified above as having bond angles near 10°. In contrast, the *6d7s* configuration of the low-lying sextet states of U$^+$ put only one electron in the antibonding 3a$_1$ MO and a *6d$_{yz}$* electron can interact with the empty H$_2$ (σ_u*) orbital to form the bonding 1b$_2$ MO. This leads to the U$^+$(H$_2$) adducts in ^{6}A$_1$, ^{6}A$_2$, ^{6}B$_1$, and ^{6}B$_2$ states at ∠HUH angles near 20°, which have deeper wells compared to the 10° adducts. Adducts at higher energies also evolve from higher energy reactant asymptotes and include those having doublet and quartet spin, Figures 5 and S1.

As the ∠HUH angle increases from the adducts, the potential energy surfaces all increase in energy as the H$_2$ bond begins to break. These surfaces eventually reach maxima near 90° as U$^+$ inserts into the H$_2$ bond. These maxima lie at energies near or above the UH$^+$ + H product asymptote. Near 30°, these surfaces cross those leading to the stable large-angle UH$_2$$^+$ intermediates having quartet and doublet spin states. As formation of these intermediates requires two singlet-coupled electrons in the in-plane *6d$_{yz}$* orbital of U$^+$ (leading to the doubly-

occupied $1b_2$ bonding MO), these surfaces correlate diabatically with highly excited U$^+$ ($5f\,^36d^2$) states. The approximate energies of these surface crossings are well below the energy of the UH$^+$ + H products and therefore should not limit the observed reactivity. From the large angle UH$_2^+$ quartet state intermediates, spin-conserving loss of an H ligand can lead to high-spin coupled UH$^+$ (^{5}I, $^5\Phi$, $^5\Delta$, $^5\Sigma^-$, $^5\Gamma$, ^{5}H) + H (^{2}S) or low-spin coupled UH$^+$ ($^3\Phi$, ^{3}I, $^3\Delta$, $^3\Sigma^-$) + H (^{2}S) products with no barrier in excess of the asymptotic energies. Likewise, formation of doublet-spin insertion intermediates could lead to low-lying triplet or singlet states of UH$^+$ in spin-conserving reactions. Overall, these surfaces show that the reaction of the experimentally formed U$^+$ (^{4}I$_{9/2}$, ^{6}L$_{11/2}$, possibly ^{6}K$_{9/2}$) cations with H$_2$ can occur via the formation of stable dihydride intermediates, although this requires coupling to surfaces evolving from excited state reactant asymptotes such that there is a barrier to formation of the inserted UH$_2^+$ intermediates. Reaction of the U$^+$ (^{4}I) ground and U$^+$ (^{6}L, ^{6}K) states are spin-conserving throughout the reaction to form UH$^+$ (^{5}I) + H (^{2}S). Both quartet and sextet reactant states could react by passing over the barriers at 90° or by coupling to quartet dihydride surfaces, which seems feasible given the large spin−orbit interactions in this heavy metal system.

DISCUSSION

UH$^+$ Electronic Ground State. As noted above, the present calculations as well as most of those in the literature find a quintet spin state as the ground state for UH$^+$, although coupling of different states and variations in the occupation of the $5f$ orbitals lead to different assignments of the Λ quantum number. It seems reasonable that the ground state assignment parallels that for UF$^+$ and UCl$^+$, which have been calculated including spin-orbit interactions at the CASPT2/CBS level by Bross and Peterson.[105] These authors comment that the order of the low-lying Ω states (and their ΛS compositions) of neutral UH is similar to that of neutral UF and UCl, where all three molecules can be considered as ionic U$^+$X$^-$. Once ionized, the additional charge on these molecules is localized on uranium such that a natural bond orbital (NBO) analysis[100-101] indicates that the natural charge on U increases from +0.85 for UF to +1.81 for UF$^+$, and from +0.76 for

UCl to +1.65 for UCl$^+$.[105] For UH$^+$, both ^{5}I and $^5\Phi$ states, NBO analyses indicate that the natural charge on U is +1.51 (calculated at the B3LYP/cc-pwCVQZ-MDF level) or +1.62 (at the CCSD(T)/cc-pwCVQZ-MDF level), thus showing a similar but slightly less ionic bond in UH$^+$ compared to UF$^+$ and UCl$^+$. Finally, Bross and Peterson found that the dominant configurations of the U center in UF$^+$ and UCl$^+$ were *5f^{3}7s* and *5f^{3}6d*,[105] as also found here for UH$^+$, Table 5, with the former dominating. As previously noted by Antonov and Heaven,[85] neither of these configurations is that of ground state U^{2+} (^{5}I$_4$, *5f^4*), but because the *7s* electron can more easily polarize away from the X$^-$ ligand, the *5f^{3}7s* state is stabilized relative to *5f^4* and *5f^{3}6d*. Overall, we conclude that the true ground state of UH$^+$ probably matches that of UF$^+$ and UCl$^+$, which Bross and Peterson assign as a Ω = 4 state derived from ^{5}I (78% UF$^+$; 66% UCl$^+$), ^{5}H (18% UF$^+$; 26% UCl$^+$), and $^5\Gamma$ (3% UF$^+$; 7% UCl$^+$) states. The ground states of UH$^+$, UF$^+$,[85,105] and UCl^{+105} all have a single bonding MO, the 1σ here, and occupy the *7s*, the 2σ here. Although Bross and Peterson[105] note that donation from the halogen atom *pπ* orbitals into empty *6dπ* orbitals can also contribute to the bonding, this effect cannot occur for UH$^+$ because the H ligand has no occupied *p*-orbitals. This conclusion seems evident from a comparison of the bond energies, 2.48 ± 0.06 eV for UH$^+$ versus 6.57 ± 0.10 eV for UF$^+$.

Presuming the three *5f* electrons in ground state U$^+$ are largely inert and core-like, the electronic structure of UH$^+$ can be compared to the hydrides of the group 3 metal cations and analogous lanthanides: Sc$^+$(^{3}D, *3d^{1}4s^1*), Y$^+$(^{1}S, *5s^2*), Gd$^+$(^{10}D, *4f^{7}5d^{1}6s^1*), La$^+$(^{3}F, *5d^2*) and Lu$^+$(^{1}S, *4f^{14}6s^2*). Predicted ground states for these metal hydride cations are ScH$^+$($^2\Delta$, $\sigma^2\delta^1$),[118] YH$^+$($^2\Sigma^+$, $\sigma^2\sigma^1$),[119-120] LaH$^+$($^2\Delta$, $\sigma^2\delta^1$),[121] GdH$^+$($^9\Sigma^-$, $\sigma^2\sigma^1$[4f^7]),[50] and UH$^+$(^{5}I, $\sigma^2\sigma^1$[5f^3]). No theoretical calculations have been performed for LuH$^+$, but we have previously pointed out that the Lu$^+$ *6s^2* ground state configuration should lead to a $^2\Sigma^+$ ($\sigma^2\sigma^1$[4f^{14}]) ground state.[40] This is in analogy with both Y$^+$ and U$^+$, where the *ns^2* ground state atomic configurations lead to $\sigma^2\sigma^1$ valence configurations in the hydride. For Y$^+$, because the bonding orbital on the metal is largely *5s*, the ground state configuration naturally leads to the nonbonding MO being σ in character with no promotion to a different state needed. For Lu$^+$ and U$^+$, the metal bonding orbital is largely the *dσ*,

such that promotion to a d^1s^1 state is needed for efficient bonding to H, while still retaining the nonbonding σ MO having ns character. The same bonding character obtains for Gd^+, where the atomic ground state is already $5d^16s^1$. In contrast, for La^+, the ground state $5d^2$ configuration leads naturally to bonding with the $d\sigma$ and occupation of a nonbonding δ MO in LaH^+. For the d^1s^1 configuration of Sc^+, the $4s$ orbital is the metal bonding orbital,[42] which also leads to a nonbonding δ MO in ScH^+.

MH^+ Thermochemistry. The BDEs (in eV) of these various ions can also be compared: $D_0(Sc^+–H) = 2.44 \pm 0.09$,[40] $D_0(Y^+–H) = 2.66 \pm 0.06$,[40] $D_0(La^+–H) = 2.48 \pm 0.09$ eV,[40] $D_0(Gd^+–H) = 2.18 \pm 0.07$,[50] and $D_0(Lu^+–H) = 2.11 \pm 0.16$,[40] as measured in guided ion beam experiments analogous to the present $D_0(U^+–H) = 2.48 \pm 0.06$. Thus, BDEs for ScH^+, YH^+, LaH^+, and UH^+ are similar, with those for GdH^+ and LuH^+ being smaller. Treating these bonds as largely covalent, variations in these BDEs can be qualitatively understood by appreciating that different orbitals are used as one moves down the periodic table (as noted above), coupled with promotion energy (E_p) arguments.[42-43] E_p is defined as the energy associated with promoting the ground level of M^+ to a state having an electronic configuration appropriate for bonding, which should involve formation of a directional and sterically unhindered metal orbital having a single electron that is spin decoupled from other electrons. As discussed previously for Sc^+, Y^+, La^+, and Lu^+,[40] which have E_p values of 0.16, 0.28, 0.26, and 1.89 eV, respectively, if one presumes that the intrinsic metal hydride BDEs are similar, the promotion energy argument helps explain why LuH^+ has a relatively weak bond compared to the other three metal hydride cations, which are more similar. Thus, with $E_p = 0.036$ eV for promotion of ground state U^+ ($5f^37s^2$) to U^+ ($5f^36d7s$) (which does not include spin decoupling), the BDE for UH^+ of 2.48 ± 0.06 eV is also similar to the thermochemistry for ScH^+, YH^+, and LaH^+. For Gd^+, we have previously assigned E_p as 0.0 eV because the ground state is $4f^75d^16s^1$,[50] however, including the spin decoupling criterion increases E_p to 0.30 eV (average energy of the ground ^{10}D and excited ^8D states, which are 0.123 and 0.481 eV after averaging over spin-orbit levels).[122] This E_p value is similar to those of Y^+ and La^+, yet the BDE for GdH^+ is closer to that of LuH^+. We have previously suggested that the

lower BDE for GdH$^+$ compared to LaH$^+$ could be a consequence of repulsive interactions between the bonding σ MO and the nonbonding σ MO for GdH$^+$ (largely the metal *6s*), whereas LaH$^+$ has a δ nonbonding MO (a pure metal *5d*). However, a similar agument does not appear to hold for either YH$^+$ nor UH$^+$, which also have σ nonbonding MOs. This observation could suggest that repulsive interactions with the *4f^7* orbitals of Gd (and also Lu), which must occupy the *4f σ*, may also be influential. It can also be realized that the nature of the bonding in LaH$^+$, GdH$^+$, LuH$^+$, and UH$^+$ may vary because the bonding MO can involve differing amounts of *sd*-hybridization, which has been shown to vary significantly across the periodic table.[123] Such variations are consistent with lanthanide contraction effects and the relative energies of the *5d* and *6s* orbitals across the lanthanide series. As is evident from the different ground state configurations of La$^+$ (*5d^2*) and Lu$^+$ (*4f^{14}6s^2*), the stability of the *6s* orbital increases with increasing number of *4f* electrons.

As noted by a reviewer (and pointed out above for UH$^+$), these molecules can alternatively be viewed as ionic, i.e., M^{2+}H$^-$. In this case, the relative BDEs should be inversely related to the second IE of M, which is much higher for Lu (14.13 eV) than the other metals considered here, consistent with the lower LuH$^+$ BDE. La and U have the lowest second IEs, 11.18 and 11.59 eV, respectively, consistent with their strong BDEs; but those for Sc, Y, and Gd are comparable: 12.80, 12.22, and 12.08 eV.[122] Thus, variations in the orbital overlaps and occupations of the nonbonding orbitals would again become influential in understanding the periodic trends.

It is also worth comparing the BDE for UH$^+$ determined here with those for other actinides, although few values exist. Other than the 2.45 ± 0.07 eV BDE for ThH$^+$ measured using GIBMS techniques,[31] only a lower limit of 0.37 ± 0.10 eV is available for PuH$^+$.[9] Promotion energy arguments and comparisons to thermochemistry for the fluorides was used to predict that D$_0$(UH$^+$) should be 2.41 ± 0.07 eV, given E_p = 0.036 eV for U$^+$.[31] This prediction is within experimental uncertainty of the 2.48 ± 0.06 eV determined here, giving credence to the promotion energy arguments. It also suggests that the three *5f* electrons do not exert an

appreciable effect on the thermochemical BDE. Notably, neither the ^{5}I nor $^5\Phi$ states of UH$^+$ occupy the *5fσ* orbital.

The SO energy correction calculated at the DK2-CASSCF-MS-CASPT2-RASSI level of theory from the difference in SO effects for UH$^+$ and U$^+$ is found to be an order of magnitude smaller compared to the estimated value obtained using calculated spectroscopic data for UF$^+$. Indeed, the calculated SO energy correction for UH$^+$ is closer to the value estimated for ThH$^+$ (~0.1 eV),[31] although smaller. One should expect the σ-bonding interactions with the hydrogen *1s* in UH$^+$ to be considerably different from those in UF$^+$, where the fluorine *2p* orbitals interact through π orbitals in addition to σ orbitals, thereby leading to the much larger bond energy.

Reaction Mechanism. As noted above, the experimental branching ratio observed in the reaction of U$^+$ + HD indicates that the reaction occurs via category 2 (direct) behavior and short-lived intermediates. In contrast, the PESs of Figure 4 find strongly bound quartet UH$_2^+$ intermediates that conceivably could lead to category 1 (statistical) behavior typical of long-lived intermediates. This contrast suggests that the coupling between the surfaces in the entrance channel (characterized by the weakly bound U$^+$(H$_2$) adducts) and those leading to the strongly bound UH$_2^+$ intermediates influences the observed reactivity. Clearly, there are apparent barriers of 0.7 – 1.2 eV where these surfaces are likely to interact (and the energies are probably higher as Figure 4 does not account for the fact that the UH bond distances can differ on the various surfaces). These barriers are similar to that calculated by Di Santo et al. for insertion of U$^+$ (^{4}I) into the C-H bond of methane, 0.59 eV.[30] Thus, the observation of category 2 (direct) behavior probably indicates that these barriers between the U$^+$(H$_2$) adducts and the inserted species lead to short-lived intermediates (i.e., when there is enough energy to form the UH$^+$ + H products, because the strongly bound UH$_2^+$ intermediates cannot be formed without passing over a barrier, the lifetime of the transient U$^+$(H$_2$) intermediates will be short). Alternatively, it is possible that reactions of U$^+$ tend to remain on the diabatic surfaces that have a barrier nearly equal to the product energy asymptote.

The reactivity of U^+ with HD can be compared with those of the transition metal and lanthanide cations that have two valence electrons: $Sc^+(^3D, 3d^14s^1)$, $Y^+(^3D, 4d^15s^1)$, $La^+(^3F, 5d^2)$, $Gd^+(^{10}D, 4f^75d^16s^1)$, and $Lu^+(^1S, 4f^{14}6s^2)$. The HD branching ratios for each of these metals are compared in Figure 5. The branching ratio of $\sigma(MH^+)/\sigma_{total}$ for Sc^+ and Gd^+ are similar to that observed here for U^+ near threshold. This is consistent with Sc^+ and Gd^+ having $(n-1)d^1ns^1$ valence configurations and suggests that the reactive U^+ state is the low-lying U^+ $(5f^36d7s)$, as indicated above by the potential energy surfaces. As the energy increases, both the Sc^+ and Gd^+ branching ratios decrease, indicating a more statistical mechanism. This can occur by coupling to low-lying $(n-1)d^2$ states, as discussed elsewhere.[40,50] In contrast, the $6d^2$ state of U^+ is much higher in energy (Table 1), such that it maintains the same branching ratio up until the bond energy of H_2 is reached. In contrast to Sc^+, Gd^+, and U^+, the branching ratio for $La^+(^3F, 5d^2)$ is very close to 0.5 (indicating statistical behavior) throughout the low-energy region below $D_0(H_2)$, consistent with its ground state configuration. Y^+ falls in between these two limits, also consistent with its $^3D(4d^15s^1)$ state mixing with its $^3F(4d^2)$ state.[40] Lu^+ shows impulsive behavior at threshold (consistent with the expected behavior for a filled $6s$ orbital) but then switches to direct behavior ($\sigma(MH^+)/\sigma_{total} \sim 0.8$), presumably because the $^1S(6s^2)$ state mixes with $^1D(5d^16s^1)$. Likewise, Th^+ starts out with impulsive characteristics, consistent with its $^2D(6d^17s^2)$ ground state but then switches to reactivity like that of Sc^+ and Gd^+, which presumably involves its low-lying $^4F(6d^27s^1)$ state. The situation for Th^+ is complicated by the fact that most low-lying levels (including the $\Omega = 3/2$ ground level) are mixtures of these two electronic configurations. The similar reaction behavior of $U^+ + HD$ to those of group 3 transition and lanthanide metal cations are consistent with the assumption that the reactivity of U^+ primarily depends on the $6d$ and $7s$ electrons, with the $5f$ electrons having little direct influence on the chemistry observed.

CONCLUSION

The kinetic energy dependent endothermic reactions of U^+ with H_2, D_2, and HD were studied using GIBMS. Analyses of the kinetic energy dependences of the cross sections in

Figures 1−3 allows the determination of $D_0(U^+−H) = 2.48 \pm 0.06$ eV. This value is considerably below other values in the literature[2,28] (although the discrepancy with previous ion beam results can be explained), but is similar to that for ThH$^+$, as predicted in that work.[31] In general, theoretical values of the UH$^+$ BDE calculated at the CCSD(T)/CBS and CASSCF-CASPT2-RASSI level are in excellent agreement with experiment, whereas B3LYP and PBE0 yield values being somewhat too high, and the M06 level of theory appreciably underestimates the BDE, Tables 3 and 5. The use of larger cc-pwCVQZ-MDF and cc-pVQZ-MDF basis sets does improve theoretical results compared to the smaller SDD-VDZ and Seg. SDD-VQZ basis sets. Branching ratios from reactions 7 and 8 indicate that the reaction proceeds via a direct mechanism, even though theory indicates there are strongly bound UH$_2^+$ intermediates. This is thought to result from the dynamics associated with barriers between the initially formed U$^+$(H$_2$) adducts and these intermediates as shown in Figure 4. Although the methods employed here restrict this work to the determination of the thermochemistry of the uranium hydride cation, it can be realized that combining this information with the ionization energies of U and UH (the latter of which is presently undetermined) would permit evaluation of the UH neutral BDE as well.

ASSOCIATED CONTENT

Supporting Information

Tables of relative energies, molecular parameters, and bond energies calculated at additional levels of theory for U$^+$, UH$^+$, and UH$_2^+$. Figure S1 shows the potential energy surfaces of UH$_2^+$ having A″ symmetry. The Supporting Information is available free of charge on the ACS Publications website at DOI: 10.1021/acs.jpca.xxxxxx.

AUTHOR INFORMATION

Corresponding Author

P. B. Armentrout: *E-mail: armentrout@chem.utah.edu. Phone: +1 (801) 581-7885. ORCID: 0000-0003-2953-6039

Author

Wibe A. de Jong: ORCID: 0000-0002-7114-8315

Notes

The authors declare no competing financial interest.

REFERENCES
(1) Choppin, G. R. Actinide speciation in the environment. *J. Radioanal. Nucl. Chem.* **2007,** *273*, 695-703.
(2) Armentrout, P. B.; Hodges, R. V.; Beauchamp, J. L. Endothermic Reactions of Uranium Ions with N_2, D_2 and CD_4. *J. Chem. Phys.* **1977,** *66*, 4683-4688.
(3) Marçalo, J.; Leal, J. P.; Pires de Matos, A. Gas phase actinide ion chemistry: activation of alkanes and alkenes by thorium cations. *Int. J. Mass Spectrom. Ion Processes* **1996,** *157/158*, 265-274.
(4) Gibson, J. K. Gas-Phase Transuranium Organometallic Chemistry: Reactions of Np^+, Pu^+, NpO^+, and PuO^+ with Alkenes. *J. Am. Chem. Soc.* **1998,** *120*, 2633-2640.
(5) Gibson, J. K. Actinide Gas-Phase Chemistry: Reactions of An^+ and AnO^+ [An = Th, U, Np, Pu, Am] with Nitriles and Butylamine. *Inorg. Chem.* **1999,** *38*, 165-173.
(6) Gibson, J. K.; Haire, R. G., Berkelium and californium organometallic ions. In *Radiochim. Acta*, 2001; Vol. 89, p 363.
(7) Gibson, J. K.; Haire, R. G.; Marçalo, J.; Santos, M.; Pires de Matos, A.; Mrozik, M. K.; Pitzer, R. M.; Bursten, B. E. Gas-Phase Reactions of Hydrocarbons with An^+ and AnO^+ (An = Th, Pa, U, Np, Pu, Am, Cm): The Active Role of 5f Electrons in Organoprotactinium Chemistry. *Organomet.* **2007,** *26*, 3947-3956.
(8) Di Santo, E.; Santos, M.; Michelini, M. C.; Marçalo, J.; Russo, N.; Gibson, J. K. Gas-Phase Reactions of the Bare Th^{2+} and U^{2+} Ions with Small Alkanes, CH_4, C_2H_6, and C_3H_8: Experimental

and Theoretical Study of Elementary Organoactinide Chemistry. *J. Am. Chem. Soc.* **2011,** *133*, 1955-1970.

(9) Marçalo, J.; Santos, M.; Gibson, J. K. Gas-Phase Reactions of Doubly Charged Actinide Cations with Alkanes and Alkenes-Probing the Chemical Activity of 5f Electrons from Th to Cm. *Phys. Chem. Chem. Phys.* **2011,** *13*, 18322-18329.

(10) Gibson, J. K., Gas-Phase Reactions of An^+ and AnO^+ [An = Th, U, Np, Pu, Am] with Halogenated Hydrocarbons [$C_{14}F_{24}$, C_3F_6, $C_2H_4Cl_2$ and $C_2H_4Br_2$]. In *Radiochim. Acta*, 1999; Vol. 84, p 135.

(11) Armentrout, P. B.; Beauchamp, J. L. Reactions of U^+ and UO^+ with O_2, CO, CO_2, COS, CS_2 and D_2O. *Chem. Phys.* **1980,** *50*, 27-36.

(12) Armentrout, P. B.; Beauchamp, J. L. Collision Induced Dissociation of UO^+ and UO_2^+ *Chem. Phys.* **1980,** *50*, 21-25.

(13) Cornehl, H. H.; Wesendrup, R.; Diefenbach, M.; Schwarz, H. A Comparative Study of Oxo-Ligand Effects in the Gas-Phase Chemistry of Atomic Lanthanide and Actinide Cations. *Chem. Eur. J.* **1997,** *3*, 1083-1090.

(14) Gibson, J. K.; Haire, R. G. Gas-Phase Chemistry of Bare and Oxo-Ligated Protactinium Ions: A Contribution to a Systematic Understanding of Actinide Chemistry. *Inorg. Chem.* **2002,** *41*, 5897-5906.

(15) Santos, M.; Marçalo, J.; Matos, A. P. d.; Gibson, J. K.; Haire, R. G. Gas-Phase Oxidation Reactions of Neptunium and Plutonium Ions Investigated via Fourier Transform Ion Cyclotron Resonance Mass Spectrometry. *J. Phys. Chem. A* **2002,** *106*, 7190-7194.

(16) Gibson, J. K. Role of Atomic Electronics in f-Element Bond Formation: Bond Energies of Lanthanide and Actinide Oxide Molecules. *J. Phys. Chem. A* **2003,** *107*, 7891-7899.

(17) Gibson, J. K.; Haire, R. G.; Santos, M.; Marcüalo, J.; Matos, A. P. d. Oxidation Studies of Dipositive Actinide Ions, An^{2+} (An = Th, U, Np, Pu, Am) in the Gas Phase: Synthesis and Characterization of the Isolated Uranyl, Neptunyl, and Plutonyl Ions $UO_2^{2+}(g)$, $NpO_2^{2+}(g)$, and $PuO_2^{2+}(g)$. *J. Phys. Chem. A* **2005,** *109*, 2768-2781.

(18) Gibson, J. K.; Haire, R. G.; Marçalo, J.; Santos, M.; Leal, J. P.; Pires de Matos, A.; Tyagi, R.; Mrozik, M. K.; Pitzer, R. M.; Bursten, B. E. FTICR/MS Studies of Gas-phase Actinide Ion Reactions: Fundamental Chemical and Physical Properties of Atomic and Molecular Actinide Ions and Neutrals. *Eur. Phys. J. D* **2007,** *45*, 133-138.

(19) Marçalo, J.; Gibson, J. K. Gas-Phase Energetics of Actinide Oxides: An Assessment of Neutral and Cationic Monoxides and Dioxides from Thorium to Curium. *J. Phys. Chem. A* **2009,** *113*, 12599-12606.

(20) de Almeida, K. J.; Duarte, H. A. Dehydrogenation of Methane by Gas-Phase Th, Th^+, and Th^{2+}: Theoretical Insights into Actinide Chemistry. *Organomet.* **2010,** *29*, 3735-3745.

(21) Infante, I.; Kovacs, A.; Macchia, G. L.; Shahi, A. R. M.; Gibson, J. K.; Gagliardi, L. Ionization Energies for the Actinide Mono- and Dioxides Series, from Th to Cm: Theory versus Experiment. *J. Phys. Chem. A* **2010,** *114*, 6007-6015.

(22) Zhou, J.; Schlegel, H. B. Ab Initio Molecular Dynamics Study of the Reaction between Th^+ and H_2O. *J. Phys. Chem. A* **2010,** *114*, 8613-8617.

(23) Cox, R. M.; Armentrout, P. B.; de Jong, W. A. Activation of CH_4 by Th^+ as Studied by Guided Ion Beam Mass Spectrometry and Quantum Chemistry. *Inorg. Chem.* **2015,** *54*, 3584-3599.

(24) Baños, A.; Harker, N.; Scott, T. B. A review of uranium corrosion by hydrogen and the formation of uranium hydride. *Corros. Sci.* **2018,** *136*, 129-147.

(25) Souter, P. F.; Kushto, G. P.; Andrews, L.; Neurock, M. Experimental and Theoretical Evidence for the Formation of Several Uranium Hydride Molecules. *J. Am. Chem. Soc.* **1997,** *119*, 1682-1687.

(26) Raab, J.; Lindh, R. H.; Wang, X.; Andrews, L.; Gagliardi, L. A Combined Experimental and Theoretical Study of Uranium Polyhydrides with New Evidence for the Large Complex $UH_4(H_2)_6$. *J. Phys. Chem. A* **2007,** *111*, 6383-6387.

(27) Straka, M.; Hrobárik, P.; Kaupp, M. Understanding Structure and Bonding in Early Actinide $6d^05f^0$ MX_6^q (M = Th−Np; X = H, F) Complexes in Comparison with Their Transition Metal $5d^0$ Analogues. *J. Am. Chem. Soc.* **2005,** *127*, 2591-2599.

(28) Moreland, P. E.; Rokop, D. J.; Stevens, C. M. Mass-spectrometric observations of uranium and plutonium monohydrides formed by ion—molecule reaction. *International Journal of Mass Spectrometry and Ion Physics* **1970,** *5*, 127-136.

(29) Sansonetti, J. E.; Martin, W. C. Handbook of Basic Atomic Spectroscopic Data. *J. Phys. Chem. Ref. Data* **2005,** *34*, 1559-2259.

(30) Di Santo, E.; Michelini, M. d. C.; Russo, N. Methane C−H Bond Activation by Gas-Phase Th^+ and U^+: Reaction Mechanisms and Bonding Analysis. *Organomet.* **2009,** *28*, 3716-3726.

(31) Cox, R. M.; Armentrout, P. B.; de Jong, W. A. Reactions of $Th^+ + H_2$, D_2, and HD Studied by Guided Ion Beam Tandem Mass Spectrometry and Quantum Chemical Calculations. *J. Phys. Chem. B* **2016,** *120*, 1601-1614.

(32) Heaven, M. C.; Barker, B. J.; Antonov, I. O. Spectroscopy and Structure of the Simplest Actinide Bonds. *J. Phys. Chem. A* **2014,** *118*, 10867-10881.

(33) Lau, K. H.; Brittain, R. D.; Hildenbrand, D. L. High temperature thermodynamic studies of some gaseous thorium fluorides. *J. Chem. Phys.* **1989,** *90*, 1158-1164.

(34) Hildenbrand, D. L.; Lau, K. H. Redetermination of the thermochemistry of gaseous UF5, UF2, and UF. *J. Chem. Phys.* **1991,** *94*, 1420-1425.

(35) Elkind, J. L.; Armentrout, P. B. Effect of Kinetic and Electronic Energy on the Reaction of V^+ with H_2, HD and D_2. *J. Phys. Chem.* **1985,** *89*, 5626-5636.

(36) Elkind, J. L.; Armentrout, P. B. Effect of Kinetic and Electronic Energy on the Reactions of Fe^+ with H_2, HD and D_2: State-Specific Cross Sections for $Fe^+(^6D)$ and $Fe^+(^4F)$. *J. Phys. Chem.* **1986,** *90*, 5736-5745.

(37) Elkind, J. L.; Armentrout, P. B. Effect of Kinetic and Electronic Energy on the Reactions of Mn^+ with H_2, HD and D_2 *J. Chem. Phys.* **1986,** *84*, 4862-4871.

(38) Elkind, J. L.; Armentrout, P. B. Effect of Kinetic and Electronic Energy on the Reactions of Cr^+ with H_2, HD and D_2. *J. Chem. Phys.* **1987,** *86*, 1868-1877.

(39) Elkind, J. L.; Armentrout, P. B. Effect of Kinetic and Electronic Energy on the Reactions of Ti^+ with H_2, HD and D_2. *Int. J. Mass Spectrom. Ion Processes* **1988,** *83*, 259-284.

(40) Elkind, J. L.; Sunderlin, L. S.; Armentrout, P. B. Periodic Trends in Chemical Reactivity: Reactions of Sc^+, Y^+, La^+, and Lu^+ with H_2, D_2, and HD. *J. Phys. Chem.* **1989,** *93*, 3151-3158.

(41) Elkind, J. L.; Armentrout, P. B. Effect of Kinetic and Electronic Energy on the Reactions of Co^+, Ni^+ and Cu^+ with H_2, HD and D_2. *J. Phys. Chem.* **1986,** *90*, 6576-6586.

(42) Elkind, J. L.; Armentrout, P. B. Transition Metal Hydride Bond Energies: First and Second Row. *Inorg. Chem.* **1986,** *25*, 1078-1080.

(43) Chen, Y.-M.; Elkind, J. L.; Armentrout, P. B. Reactions of Ru^+, Rh^+, Pd^+, and Ag^+ with H_2, HD and D_2. *J. Phys. Chem.* **1995,** *99*, 10438-10445.

(44) Sievers, M. R.; Chen, Y.-M.; Elkind, J. L.; Armentrout, P. B. Reactions of Y^+, Zr^+, Nb^+, and Mo^+ with H_2, HD, and D_2. *J. Phys. Chem.* **1996,** *100*, 54-62.

(45) Zhang, X.-G.; Armentrout, P. B. Reactions of Pt^+ with H_2, D_2, and HD: Effect of Lanthanide Contraction on Reactivity and Thermochemistry. *J. Chem. Phys.* **2002,** *116*, 5565-5573.

(46) Zhang, X.-G.; Rue, C.; Shin, S.-Y.; Armentrout, P. B. Reactions of Ta^+ and W^+ with H_2, D_2, and HD: Effect of Lanthanide Contraction and Spin-Orbit Interactions on Reactivity and Thermochemistry. *J. Chem. Phys.* **2002,** *116*, 5574-5583.

(47) Hinton, C. S.; Armentrout, P. B. Guided Ion Beam and Theoretical Study of the Reactions of Hf^+ with H_2, D_2, and HD *J. Chem. Phys.* **2010,** *133*, 124307.

(48) Hinton, C. S.; Citir, M.; Armentrout, P. B. Guided Ion Beam and Theoretical Study of the Reactions of Os^+ with H_2, D_2, and HD. *J. Chem. Phys.* **2011,** *135*, 234302.

(49) Li, F.-X.; Liu, F.; Armentrout, P. B. Guided Ion Beam and Theoretical Study of the Reactions of Au^+ with H_2, D_2, and HD *J. Chem. Phys.* **2011,** *134*, 024310.

(50) Demireva, M.; Armentrout, P. B. Activation of H_2 by Gadolinium Cation (Gd^+): Bond Energy of GdH^+ and Mechanistic Insights from Guided Ion Beam and Theoretical Studies. *J. Phys. Chem. A* **2018,** *122*, 750-761.

(51) Demireva, M.; Armentrout, P. B. Samarium Cation (Sm^+) Reactions with H_2, D_2, and HD: SmH^+ Bond Energy and Mechanistic Insights from Guided Ion Beam and Theoretical Studies *J. Chem. Phys.* **2018,** *149*, 164304.

(52) Ervin, K. M.; Armentrout, P. B. Translational Energy Dependence of $Ar^+ + XY \rightarrow ArX^+ + Y$ ($XY = H_2$, D_2, HD) from Thermal to 30 eV c.m. *J. Chem. Phys.* **1985,** *83*, 166-189.

(53) Loh, S. K.; Hales, D. A.; Lian, L.; Armentrout, P. B. Collision-Induced Dissociation of Fe_n^+ ($n = 2 - 10$) with Xe: Ionic and Neutral Iron Cluster Binding Energies. *J. Chem. Phys.* **1989,** *90*, 5466-5485.

(54) Schultz, R. H.; Armentrout, P. B. Reactions of N_4^+ with Rare Gases from Thermal to 10 eV c.m.: Collision-Induced Dissociation, Charge Transfer, and Ligand Exchange. *Int. J. Mass Spectrom. Ion Processes* **1991,** *107*, 29-48.

(55) Teloy, E.; Gerlich, D. Integral Cross Sections for Ion-Molecule Reactions. 1. The Guided Beam Technique. *Chem. Phys.* **1974,** *4*, 417-427.

(56) Gerlich, D., Inhomogeneous rf Fields: A Versatile Tool for the Study of Processes with Slow Ions. In *Adv. Chem. Phys.*, Ng, C.-Y.; Baer, M., Eds. Wiley: 1992; Vol. 82, pp 1-176.

(57) Daly, N. R. Scintillation Type Mass Spectrometer Ion Detector. *Rev. Sci. Instrum.* **1960,** *31*, 264-267.

(58) Chantry, P. J. Doppler Broadening in Beam Experiments. *J. Chem. Phys.* **1971,** *55*, 2746-2759.

(59) Lifshitz, C.; Wu, R. L. C.; Tiernan, T. O.; Terwilliger, D. T. Negative Ion-molecule Reactions of Ozone and Their Implications on the Thermochemistry of O_3^-. *J. Chem. Phys.* **1978,** *68*, 247-260.

(60) Haynes, C. L.; Armentrout, P. B. Thermochemistry and Structures of $CoC_3H_6^+$: Metallacycle and Metal-Alkene Isomers. *Organomet.* **1994,** *13*, 3480-3490.

(61) Kickel, B. L.; Armentrout, P. B. Guided Ion Beam Studies of the Reactions of Mn^+, Cu^+, and Zn^+ with Silane. M^+-SiH_x ($x = 0 - 3$) Bond Energies. *J. Phys. Chem* **1995,** *99*, 2024-2032.

(62) Kickel, B. L.; Armentrout, P. B. Guided Ion Beam Studies of the Reactions of Group 3 Metal Ions (Sc^+, Y^+, La^+, and Lu^+) with Silane. Electronic State Effects, Comparison to Reactions with Methane, and M^+-SiH_x ($x = 0 - 3$) Bond Energies. *J. Am. Chem. Soc.* **1995,** *117*, 4057-4070.

(63) Clemmer, D. E.; Chen, Y.-M.; Khan, F. A.; Armentrout, P. B. State-Specific Reactions of Fe^+(a^6D, a^4F) with D_2O and Reactions of FeO^+ with D_2. *J. Phys. Chem.* **1994,** *98*, 6522-6529.

(64) Kickel, B. L.; Armentrout, P. B. Reactions of Fe^+, Co^+ and Ni^+ with Silane. Electronic State Effects, Comparison to Reactions with Methane, and M^+-SiH_x ($x = 0 - 3$) Bond Energies. *J. Am. Chem. Soc.* **1995,** *117*, 764-773.

(65) Blaise, J.; Wyart, J.-F. *Energy Levels and Atomic Spectra of Actinides*. Paris, 1992.

(66) Armentrout, P. B. The Kinetic Energy Dependence of Ion-Molecule Reactions: Guided Ion Beams and Threshold Measurements. *Int. J. Mass Spectrom.* **2000,** *200*, 219-241.

(67) Chesnavich, W. J.; Bowers, M. T. Theory of Translationally Driven Reactions. *J. Phys. Chem* **1979,** *83*, 900-905.

(68) Muntean, F.; Armentrout, P. B. Guided Ion Beam Study of Collision-Induced Dissociation Dynamics: Integral and Differential Cross Sections. *J. Chem. Phys.* **2001,** *115*, 1213-1228.

(69) Schultz, R. H.; Crellin, K. C.; Armentrout, P. B. Sequential Bond Energies of $Fe(CO)_x^+$ ($x = 1 - 5$): Systematic Effects on Collision-Induced Dissociation Measurements. *J. Am. Chem. Soc.* **1991,** *113*, 8590-8601.

(70) Armentrout, P. B.; Simons, J. Understanding Heterolytic Bond Cleavage. *J. Am. Chem. Soc.* **1992,** *114*, 8627-8633.

(71) Weber, M. E.; Elkind, J. L.; Armentrout, P. B. Kinetic Energy Dependence of Al^+ + O_2 → AlO^+ + O. *J. Chem. Phys.* **1986,** *84*, 1521-1529.

(72) Frisch, M. J.; Trucks, G. W.; Schlegel, H. B.; Scuseria, G. E.; Robb, M. A.; Cheeseman, J. R.; Scalmani, G.; Barone, V.; Petersson, G. A.; Nakatsuji, H., et al. *Gaussian 16, Revision A.03*, Gaussian, Inc.: Wallingford CT, 2016.

(73) Peterson, K. A. Correlation consistent basis sets for actinides. I. The Th and U atoms. *J. Chem. Phys.* **2015,** *142*, 074105.

(74) Weigand, A.; Cao, X.; Hangele, T.; Dolg, M. Relativistic Small-Core Pseudopotentials for Actinium, Thorium, and Protactinium. *J. Phys. Chem. A* **2014,** *118*, 2519-2530.

(75) Dunning, T. H. Gaussian basis sets for use in correlated molecular calculations. I. The atoms boron through neon and hydrogen. *J. Chem. Phys.* **1989,** *90*, 1007-1023.

(76) Feller, D. The Role of Databases in Support of Computational Chemistry Calculations. *J. Comput. Chem.* **1996,** *17*, 1571-1586.

(77) Schuchardt, K. L.; Didier, B. T.; Elsethagen, T.; Sun, L.; Gurumoorthi, V.; Chase, J.; Li, J.; Windus, T. L. Basis Set Exchange: A Community Database for Computational Sciences. *J. Chem. Inf. Model.* **2007,** *47*, 1045-1052.

(78) Cao, X.; Dolg, M.; Stoll, H. Valence Basis Sets for Relativistic Energy-consistent Small-core Actinide Pseudopotentials. *J. Chem. Phys.* **2003,** *118*, 487-496.

(79) Douglas, M.; Kroll, N. M. Quantum Electrodynamical Corrections to the Fine Structure of Helium. *Ann. Phys. (N. Y.)* **1974,** *82*, 89-155.

(80) Hess, B. A. Applicability of the no-pair equation with free-particle projection operators to atomic and molecular structure calculations. *Phys. Rev. A* **1985,** *32*, 756-763.

(81) Hess, B. A. Relativistic electronic-structure calculations employing a two-component no-pair formalism with external-field projection operators. *Phys. Rev. A* **1986,** *33*, 3742-3748.

(82) Jansen, G.; Hess, B. A. Revision of the Douglas-Kroll transformation. *Phys. Rev. A* **1989,** *39*, 6016-6017.

(83) de Jong, W. A.; Harrison, R. J.; Dixon, D. A. Parallel Douglas-Kroll Energy and Gradients in NWChem: Estimating Scalar Relativistic Effects using Douglas-Kroll Contracted Basis Sets. *J. Chem. Phys.* **2001,** *114*, 48-53.

(84) Barysz, M.; Sadlej, A. J. Two-component methods of relativistic quantum chemistry: from the Douglas–Kroll approximation to the exact two-component formalism. *Journal of Molecular Structure: THEOCHEM* **2001,** *573*, 181-200.

(85) Antonov, I. O.; Heaven, M. C. Spectroscopic and Theoretical Investigations of UF and UF$^+$. *J. Phys. Chem. A* **2013,** *117*, 9684-9694.

(86) Karton, A.; Martin, J. M. L. Comment on: "Estimating the Hartree–Fock limit from finite basis set calculations" [Jensen F (2005) Theor Chem Acc 113:267]. *Theor. Chem. Acct.* **2006,** *115*, 330-333.

(87) Martin, J. M. L. Ab initio Total Atomization Energies of Small Molecules - Towards the Basis Set Limit. *Chem. Phys. Lett.* **1996,** *259*, 669-678.

(88) Feller, D.; Peterson, K. A.; Hill, J. G. On the effectiveness of CCSD(T) complete basis set extrapolations for atomization energies. *J. Chem. Phys.* **2011,** *135*, 044102.

(89) Becke, A. D. Density-functional Thermochemistry. III. The Role of Exact Exchange. *J. Chem. Phys.* **1993,** *98*, 5648-5652.

(90) Lee, C.; Yang, W.; Parr, R. G. Development of the Colle-Salvetti Correlation-Energy Formula into a Functional of the Electron Density. *Phys. Rev. B* **1988,** *37*, 785-789.

(91) Zhao, Y.; Truhlar, D. G. The M06 Suite of Density Functionals for Main Group Thermochemistry, Thermochemical Kinetics, Noncovalent Interactions, Excited States, and Transition Elements: Two New Functionals and Systematic Testing of Four M06-Class Functionals and 12 Other Functionals. *Theor. Chem. Acc.* **2008,** *120*, 215-241.

(92) Adamo, C.; Barone, V. Toward Reliable Density Functional Methods Without Adjustable Parameters: The PBE0 Model. *J. Chem. Phys.* **1999,** *110*, 6158-6170.

(93) Perdew, J. P.; Ernzerhof, M.; Burke, K. Rationale for Mixing Exact Exchange with Density Functional Approximations. *J. Chem. Phys.* **1996,** *105*, 9982-9985.

(94) Averkiev, B. B.; Mantina, M.; Valero, R.; Infante, I.; Kovacs, A.; Truhlar, D. G.; Gagliardi, L. How Accurate are Electronic Structure Methods for Actinoid Chemistry? *Theor. Chem. Acct.* **2011,** *129*, 657-666.

(95) Raghavachari, K.; Trucks, G. W.; Pople, J. A.; Head-Gordon, M. A Fifth-order Perturbation Comparison of Electron Correlation Theories. *Chem. Phys. Lett.* **1989,** *157*, 479-483.

(96) Kucharski, S. A.; Bartlett, R. J. Noniterative Energy Corrections Through Fifth-order to the Coupled Cluster Singles and Doubles Method. *J. Chem. Phys.* **1998,** *108*, 5243-5254.

(97) Scuseria, G. E.; Lee, T. J. Comparison of Coupled-cluster Methods Which Include the Effects of Connected Triple Excitations. *J. Chem. Phys.* **1990,** *93*, 5851-5855.

(98) Bozkaya, U.; Schaefer, H. F. Symmetric and Asymmetric Triple Excitation Corrections for the Orbital-optimized Coupled-cluster Doubles Method: Improving Upon CCSD(T) and CCSD(T)Λ: Preliminary Application. *J. Chem. Phys.* **2012,** *136*, 204114.

(99) Foresman, J. B.; Frisch, A. E. *Exploring Chemistry with Electronic Structure Methods.* 2nd ed.; Gaussian, Inc.: Pittsburgh, PA, 1996.

(100) Foster, J. P.; Weinhold, F. Natural Hybrid Orbitals. *J. Am. Chem. Soc.* **1980,** *102*, 7211-7218.

(101) Glendening, E. D.; Reed, A. E.; Carpenter, J. E.; Weinhold, F. *NBO Version 3.1*, Gaussian Inc.: Pittsburgh, 2003.

(102) Roos, B. O.; Taylor, P. R.; Sigbahn, P. E. M. A complete active space SCF method (CASSCF) using a density matrix formulated super-CI approach. *Chem. Phys.* **1980,** *48*, 157-173.

(103) Sauri, V.; Serrano-Andrés, L.; Shahi, A. R. M.; Gagliardi, L.; Vancoillie, S.; Pierloot, K. Multiconfigurational Second-Order Perturbation Theory Restricted Active Space (RASPT2) Method for Electronic Excited States: A Benchmark Study. *J. Chem. Theory Comput.* **2011,** *7*, 153-168.

(104) Malmqvist, P. Å.; Roos, B. O.; Schimmelpfennig, B. The restricted active space (RAS) state interaction approach with spin–orbit coupling. *Chem. Phys. Lett.* **2002,** *357*, 230-240.

(105) Bross, D. H.; Peterson, K. A. Theoretical spectroscopy study of the low-lying electronic states of UX and UX^+, X = F and Cl. *J. Chem. Phys.* **2015,** *143*, 184313.

(106) Dolg, M.; Cao, X. Accurate Relativistic Small-Core Pseudopotentials for Actinides. Energy Adjustment for Uranium and First Applications to Uranium Hydride. *J. Phys. Chem. A* **2009,** *113*, 12573-12581.

(107) Ruscic, B.; Pinzon, R. E.; Morton, M. L.; von Laszevski, G.; Bittner, S. J.; Nijsure, S. G.; Amin, K. A.; Minkoff, M.; Wagner, A. F. Introduction to Active Thermochemical Tables: Several "Key" Enthalpies of Formation Revisited. *J. Phys. Chem. A* **2004,** *108*, 9979-9997.

(108) Ruscic, B.; Bross, D. H. Active Thermochemical Tables (ATcT) values based on ver. 1.122e of the Thermochemical Network. available at ATcT.anl.gov (accessed 10/15/19).

(109) Armentrout, P. B. Periodic trends in the reactions of atomic ions with molecular hydrogen. *Int. Rev. Phys. Chem.* **1990,** *9*, 115-148.

(110) Armentrout, P. B. Isotope Effects in the Reactions of Atomic Ions with H_2, D_2, and HD. *ACS Symp. Series* **1992,** *502*, 194-209.

(111) Peng, D.; Liu, W.; Xiao, Y.; Cheng, L. Making four- and two-component relativistic density functional methods fully equivalent based on the idea of "from atoms to molecule". *J. Chem. Phys.* **2007,** *127*, 104106.

(112) Cao, X.; Moritz, A.; Dolg, M. All-electron Douglas–Kroll–Hess and pseudopotential study on the low-lying states of uranium hydride UH. *Chem. Phys.* **2008,** *343*, 250-257.

(113) Balasubramanian, K.; Siekhaus, W. J.; McLean, W. Potential Energy Surfaces for the Uranium Hydriding Reaction. *J. Chem. Phys.* **2003,** *119*, 5889-5900.

(114) Lefebvre-Brion, H.; Field, R. W. *The Spectra and Dynamics of Diatomic Molecules.* Elsevier: Amsterdam, 2004.

(115) Krauss, M.; Stevens, W. J. Electronic structure of UH, UF, and their ions. *J. Comput. Chem.* **1983,** *4*, 127-135.

(116) Di Santo, E.; Michelini, M. C.; Russo, N. Activation of Ethane C−H and C−C Bonds by Gas Phase Th^+ and U^+: A Theoretical Study. *J. Phys. Chem. A* **2009,** *113*, 14699-14705.

(117) Meftah, A.; Sabri, M.; Wyart, J.-F.; Tchang-Brillet, W.-Ü. L. Spectrum of Singly Charged Uranium (U II): Theoretical Interpretation of Energy Levels, Partition Function and Classified Ultraviolet Lines. *Atoms* **2017,** *5*, 24.

(118) Alvarado-Swaisgood, A. E.; Harrison, J. F. Electronic and geometric structures of scandium hydride cations (ScH^+ and ScH_2^+). *J. Phys. Chem.* **1985,** *89*, 5198-5202.

(119) Das, K. K.; Balasubramanian, K. Potential Energy Surfaces for YH_2^+ and ZrH_2^+. *J. Chem. Phys.* **1989,** *91*, 2433-2442.

(120) Pettersson, L. G. M.; Bauschlicher, C. W.; Langhoff, S. R.; Partridge, H. Positive ions of the first- and second-row transition metal hydrides. *J. Chem. Phys.* **1987,** *87*, 481-492.

(121) Balasubramanian, K.; Das, K. K. Potential Energy Surfaces of LaH^+ and LaH_2^+. *J. Chem. Phys.* **1991,** *94*, 3722.

(122) Kramida, A.; Ralchenko, Y.; Reader, J.; Team, N. A. NIST Atomic Spectra Database (ver. 5.7.1), [Online]. Available: http://physics.nist.gov/asd 2012. (accessed Nov 1, 2019).

(123) Ohanessian, G.; Brusich, M. J.; Goddard III, W. A. Theoretical Study of Transition-metal Hydrides. 5. HfH^+ through HgH^+, BaH^+, and LaH^+. *J. Am. Chem. Soc.* **1990,** *112*, 7179-7189.

Table 1. Fitting parameters of eq 1 for the indicated reaction cross section.

Reaction	σ_0	n	E_0 (eV)	$D_0(U^+-H)$
$U^+ + H_2 \rightarrow UH^+ + H$	5.8 ± 1.7	1.5 ± 0.2	2.05 ± 0.13	2.43 ± 0.13
$U^+ + D_2 \rightarrow UD^+ + D$	6.0 ± 1.0	1.5 ± 0.2	2.08 ± 0.08	2.45 ± 0.08[a]
$U^+ + HD \rightarrow UH^+ + D$	3.7 ± 1.9	1.6 ± 0.2	2.07 ± 0.10	2.45 ± 0.10
$U^+ + HD \rightarrow UD^+ + H$	2.5	1.3 ± 0.4	0.852	2.57 ± 0.10[a]

[a] Values derived from reactions forming UD^+ include a zero-point energy correction of -0.029 eV.

Table 2. Comparison of theoretically computed excited state energies (eV) of U^+ to experimental values.[a]

U^+	Experimental[b]	CCSD(T)	B3LYP	M06	PBE0
^4I ($5f^37s^2$)	0.00	0.00 (0.00)	0.00	0.00	0.00
^6H ($5f^36d7s$)	0.42	0.49 (0.23)	0.48	1.27	0.14
^6I ($5f^47s$)	0.46	0.74 (1.14)	0.31	1.15	0.02
^6K ($5f^36d7s$)	0.47	0.55 (0.26)	0.51	1.45	0.17
^6L ($5f^36d7s$)	0.50	0.61 (0.34)	0.55	1.59	0.21
^6M ($5f^36d^2$)	2.23	1.55 (0.91)	1.62	2.24	1.16

[a] Calculated using cc-pwCVQZ-MDF basis set. Values in parentheses were calculated without the $5s$ and $5p$ electrons frozen.

[b] Experimental energies are averaged over all spin-orbit levels and are taken from Refs. [29,65].

Table 3. Calculated spin-orbit correction for U^+, UH^+, and $D_0(U^+-H)$ (eV) at the CASSCF+ CASPT+RASSI level of theory using the DK2 Hamiltonian. The results in the last row are the

estimated bond energies at the optimized bond length for both the spin-free and spin-orbit calculations.

ᵃ Calculated values in parentheses includes a zero-point energy correction of 0.099 eV.

Table 4. Molecular parameters and calculated relative energies (eV) for ground and excited states of UH$^+$.[a]

state	configuration	r(U$^+$-H) (Å)	ν (cm^{-1})	Energy (eV)	
				B3LYP	CCSD(T)[b]
$^5\Phi$	$1\sigma^2 2\sigma[\pi^2\varphi]$	1.972	1595	0.000 (0.381)	0.000 (0.384)
^{5}I	$1\sigma^2 2\sigma[\pi\delta\varphi]$	1.974	1593	0.009 (0.000)	0.006 (0.000)
$^5\Sigma^-$	$1\sigma^2 2\sigma[\sigma\delta^2/\sigma\varphi^2]^c$	1.990	1588	0.077 (0.848)	0.034 (0.808)
$^5\Delta$	$1\sigma^2 2\sigma[\pi^2\delta/\delta\varphi^2]^c$	1.971	1600	0.041 (0.552)	0.069 (0.583)
^{5}I/Γ	$1\sigma^2 2\sigma[\pi\delta\varphi/\sigma\pi\varphi]^c$	1.977	1591	0.086 (0.077)	0.086 (0.080)
^{5}H	$1\sigma^2 2\sigma[\sigma\delta\varphi]$	1.989	1588	0.146 (0.267)	0.112 (0.236)
$^3\Phi$	$1\sigma^2 2\sigma[\pi^2\varphi/\delta^2\varphi]^c$	1.972	1588	0.289 (0.865)	0.236 (0.815)
^{3}I	$1\sigma^2 2\sigma[\pi\delta\varphi]$	1.973	1588	0.293 (0.674)	0.239 (0.623)
$^3\Sigma^-$	$1\sigma^2 2\sigma[\sigma\delta^2/\sigma\varphi^2]^c$	1.981	1580	0.336 (1.107)	0.263 (1.037)
$^3\Delta$	$1\sigma^2 2\sigma[\pi^2\delta/\delta\varphi^2]^c$	1.971	1591	0.322 (0.963)	0.286 (0.930)
$^3\Phi$	$1\sigma^2 2\sigma[\pi^2\varphi]$	1.968	1603	0.835 (1.411)	0.824 (1.403)
$^1\Sigma^-$	$1\sigma^2 2\sigma[\sigma\delta^2/\sigma\varphi^2]^c$	1.978	1601	0.979 (1.750)	0.879 (1.653)
^{1}I	$1\sigma^2 2\sigma[\pi\delta\varphi]$	1.969	1600	0.927 (1.698)	0.910 (1.684)
$^1\Phi$	$1\sigma^2 2\sigma[\pi^2\varphi]$	1.967	1597	0.947 (1.718)	0.916 (1.690)
^{1}I	$1\sigma^2 2\sigma[\pi\delta\varphi]$	1.970	1603	1.145 (1.916)	1.119 (1.893)
$^3\Delta$	$1\sigma^2 1\delta[\sigma\delta^2/\sigma\varphi^2]^c$	2.021	1512	1.255 (1.851)^d	1.176 (1.775)^d

[a] Structures optimized at B3LYP/cc-pwCVQZ-MDF/aug-cc-pVQZ. Frequencies scaled by 0.989. Energies are relative to the ground state (level) and include zero-point corrections. Values including spin-orbit corrections to the lowest level of each state using A = 0.065 eV are given in parentheses.
[b] Single point energy using B3LYP/cc-pwCVQZ-MDF/aug-cc-pVQZ optimized structures.
[c] Configurations of mixed character according to an NBO analysis are indicated by / with the leading configuration listed first.
[d] Includes a spin-orbit correction for the 1δ orbital of 0.175 eV.

Table 5. Theoretical results for ground state UH$^+$ (^{5}I).[a]

Basis set	r(U$^+$-H) (Å)[b]	v (cm^{-1})[b]	D$_0$(U$^+$-H) (eV)		
			CCSD(T)[c]	B3LYP	PBE0
SDD-VDZ-MWB/6-311+G(3pd)	1.962	1609	2.32 (*2.11*)	2.54 (*2.33*)	2.65 (*2.44*)
Seg. SDD-VQZ-MWB/6-311+G(3pd)	1.960	1612	2.30 (*2.09*)	2.52 (*2.35*)	2.67 (*2.46*)
ANO-VQZ-MWB/6-311+G(3pd)	1.960	1608	2.29 (*2.08*)	2.54 (*2.33*)	2.65 (*2.44*)
ANO-VQZ-MDF/6-311+G(3pd)	1.970	1602	2.30 (*2.09*)	2.54 (*2.33*)	2.66 (*2.45*)
CBS-cc-pwCVXZ-MDF/aug-cc-pVXZ[d]	1.974	1594	2.40 (*2.19*)	2.53 (*2.32*)	2.66 (*2.45*)
CBS-cc-pwCVXZ-MDF/cc-pVXZ[d]	1.974	1593	2.39 (*2.18*)	2.52 (*2.31*)	2.66 (*2.45*)
CBS-cc-pVXZ-MDF/aug-cc-pVXZ[d]	1.974	1593	2.36 (*2.15*)	2.52 (*2.31*)	2.65 (*2.44*)
CBS-cc-pVXZ-DK3[d,e]			2.45 (*2.24*)	2.55 (*2.34*)	2.70 (*2.49*)
CBS-cc-pwCVXZ-DK3[d,e]			2.43 (*2.22*)	2.55 (*2.34*)	2.70 (*2.49*)

[a] Calculated from structures optimized using the indicated basis sets (U$^+$ basis set – ECP/H basis set) at the respective level of theory (except for CCSD(T) and all-electron calculations) relative to U$^+$ + H. BDE values include a spin-orbit correction of either -0.074 (roman) or -0.281 (italics) eV.

[b] From B3LYP optimized structures.

[c] Single point energy using B3LYP optimized structures and zero-point corrections.

[d] Complete basis set limit extrapolated using Eqs. 4 and 5. Bond lengths and vibrational frequencies from results obtained using the associated VQZ basis sets.

[e] Single point energy from B3LYP/cc-pwCVQZ-MDF/aug-cc-pVQZ optimized structure.

Table 6. Calculated molecular parameters and relative energies for ground and excited states of UH_2^+.[a]

State[b]	Configuration	$r(U^+-H)$ (Å)[c]	$\angle HUH$ (°)[c]	Relative energies (eV)	
				CCSD(T)	B3LYP
$1\ ^4A_1$	$(1a_1)^2(1b_2)^2[1a_2{}^11b_1{}^12b_2{}^1]$	1.997	97.4	0.00 (-0.538)[d]	0.00 (-0.617)[d]
$4\ ^4B_2$	$(1a_1)^2(3a_1)^2[1b_1{}^12b_1{}^12b_2{}^1]$	*4.010*	*10.6*	*0.517*	*0.615*
$1\ ^2B_2$	$(1a_1)^2(1b_2)^2[1b_1{}^12b_1{}^12b_2{}^1]$	1.993	97.3	0.720	0.728
$1\ ^6B_1$	$(1a_1)^2(1b_2)^1(3a_1)^1[1b_1{}^12a_1{}^12b_2{}^1]$	*2.322*	*19.7*	*0.729*	*0.699*
$5\ ^4B_2$	$(1a_1)^2(1b_2)^1(3a_1)^1[1a_2{}^11b_1{}^12b_2{}^1]$	*2.329*	*19.6*	*1.074*	*1.101*
$1\ ^2A_1$	$(1a_1)^2(3a_1)^2[1b_1{}^12b_1{}^12b_2{}^1]$	*3.988(3)*[e]	*10.7*	*1.306*	*1.381*
$2\ ^2A_2$	$(1a_1)^2(1b_2)^1(3a_1)^1[1b_1{}^12b_2{}^13b_2{}^1]$	*2.255(9)*[e]	*20.9*	*1.316*	*1.364*
$6\ ^4A_2$	$(1a_1)^2(2a_2)^1(3a_1)^1[1a_2{}^11b_1{}^12b_2{}^1]$	*3.698*	*11.6*	*1.455*	*1.609*
$3\ ^6A_1$	$(1a_1)^2(1b_2)^1(3b_1)^1[1a_1{}^11b_1{}^12b_2{}^1]$	*2.230*	*21.0*	f	*1.627*
$4\ ^6A_1$	$(1a_1)^2(1b_2)^1(2a_2)^1[1b_1{}^12b_2{}^13b_2{}^1]$	*2.282*	*20.5*	*1.684*	*1.827*
$1\ ^4\Gamma$	$1\sigma^22\sigma^1[\sigma^2\pi^1\varphi^1]$	1.970	180.0	1.752	1.607
$6\ ^4A_1$	$(1a_1)^2(1b_2)^2(2a_2)^1[1a_2{}^12a_1{}^1]$	1.929	99.2	1.759	2.041
$7\ ^4B_1$	$(1a_1)^2(1b_2)^2(2a_2)^1[1a_2{}^11b_1{}^1]$	1.926	93.8	1.769	2.052
$8\ ^4A_2$	$(1a_1)^2(1b_2)^1(2a_2)^1[1a_2{}^11b_1{}^12a_1{}^1]$	*2.233*	*22.0*	*2.161*	*2.254*
$1\ ^6\Phi$	$1\sigma^22\sigma^1[\sigma^1\pi^2\varphi^1]$	2.124	180.0	2.488	2.207
$5\ ^6A_1$	$(1a_1)^2(3a_1)^1[1b_1{}^12b_1{}^12b_2{}^13b_2{}^1]$	2.126	155.5	2.574	2.327
$1\ ^4\Phi$	$1\sigma^22\sigma^1[\sigma^1\pi^2\varphi^1]$	2.139	180.0	2.640	2.366
$8\ ^4B_1$	$(1a_1)^2(3a_1)^1[1a_2{}^11b_1{}^12b_1{}^12b_2{}^1]$	2.160	166.7	2.875	2.640

ᵃ Single point energies of B3LYP/cc-pwCVQZ-MDF/aug-cc-pVQZ optimized structures. Values in italics distinguish minima found at small ∠HUH angles. Only states with B3LYP energies below 3 eV are included here.

ᵇ States are named on the basis of all states included in Table S4, such that some lower numbers are not included here.

ᶜ From B3LYP/cc-pwCVQZ-MDF/aug-cc-pVQZ optimized structures.

ᵈ Values in parentheses are relative to U^+ (^4I) + H_2.

ᵉ The two bond lengths differ slightly in the final decimal place as indicated by the number in parentheses, but orbitals are still assigned according to C_{2v} symmetry.

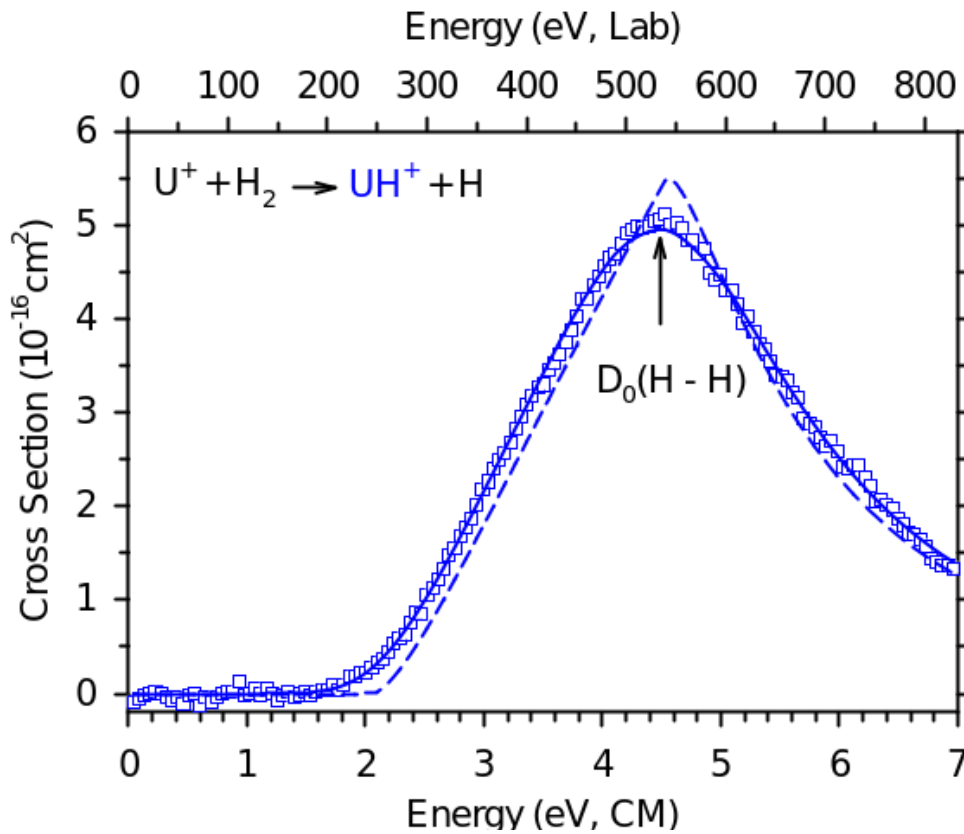ᶠ Collapses to a lower energy state.

Figure Captions

Figure 1. Cross sections for the reaction between U^+ and H_2 as a function of energy in the center-of-mass (lower x-axis) and laboratory (upper x-axis) frames. The model of eq 1 with parameters from the Table 1 is shown as a dashed line and the solid line shows the model convoluted over the kinetic energy and internal energy distributions of reactants. The arrow indicates $D_0(H_2)$ at 4.478 eV.

Figure 2. Cross sections for the reaction between U^+ and D_2 as a function of energy in the center-of-mass (lower x-axis) and laboratory (upper x-axis) frames. Results from the present work are shown by red symbols, whereas black circles provide results from Armentrout, Hodges, and Beauchamp, ref. [2]. The model of eq 1 with parameters from the Table 1 is shown as a dashed line and the solid line shows the model convoluted over the kinetic energy and internal energy distributions of reactants. The arrow indicates $D_0(D_2)$ at 4.556 eV.

Figure 3. Cross sections for the reaction between U^+ and HD as a function of energy in the center-of-mass (lower x-axis) and laboratory (upper x-axis) frames. The model of eq 1 with parameters from the Table 1 is shown as a dashed line and the solid line shows the model convoluted over the kinetic energy and internal energy distributions of reactants. The arrow indicates $D_0(HD)$ at 4.514 eV.

Figure 4. B3LYP/Seg. SDD-VQZ-MWB/6-311+(3pd) relaxed potential energy surface scan calculations of the $U^+ + H_2$ reaction surfaces having A′ symmetry as a function of the $\angle HU^+H$ bond angle in degrees. The energies are relative to U^+ (^4I, $5f\,^37s^2$) + H_2. Doublet, quartet, and sextet surfaces are represented by red, black, and blue lines, respectively, with solid lines for A_1 surfaces and dashed lines for B_2 surfaces. See Figure S1 for similar A″ surfaces. Horizontal thick lines at 0 and 180 degrees indicate the calculated relative energies of ground and excited state reactants and products. At the top, structures of UH_2^+ intermediates at 10.6, 97.4, and 180° are shown.

Figure 5. Product branching fractions ($\sigma_{MH+}/\sigma_{Total}$) for reactions of Sc^+ (cyan diamonds), Y^+ (purple triangles), La^+ (yellow circles), Gd^+ (red squares), Lu^+ (black solid circles), Th^+ (blue circles), U^+ (green circles) with HD as a function of kinetic energy in the CM frame.
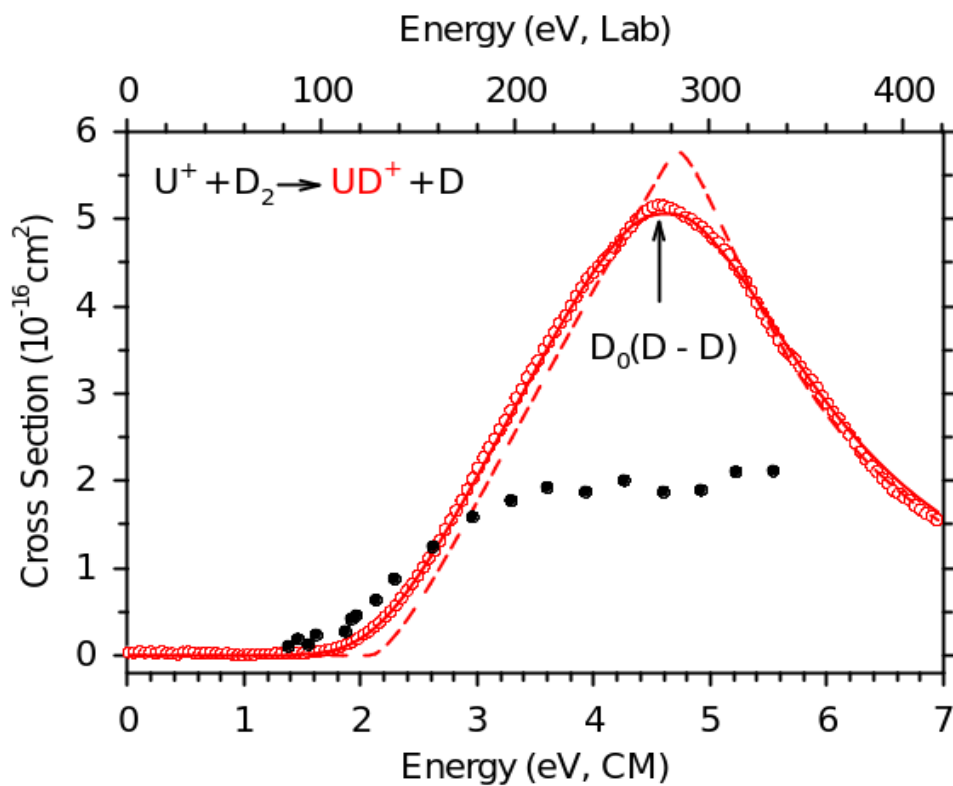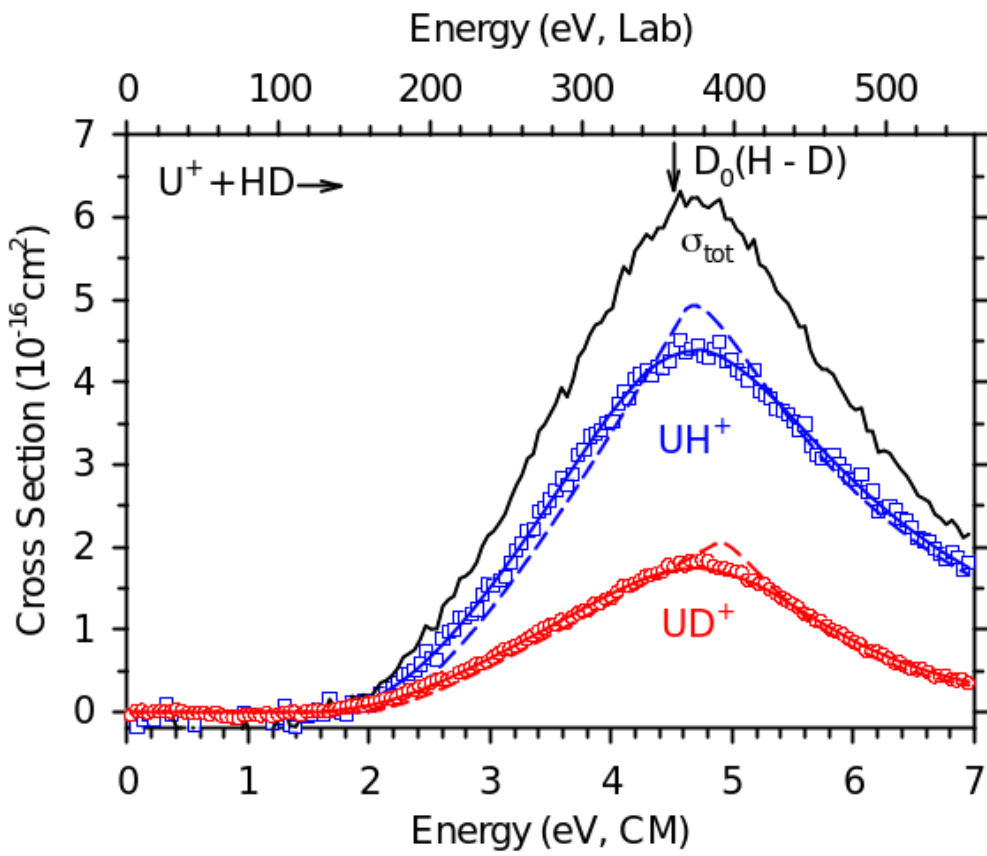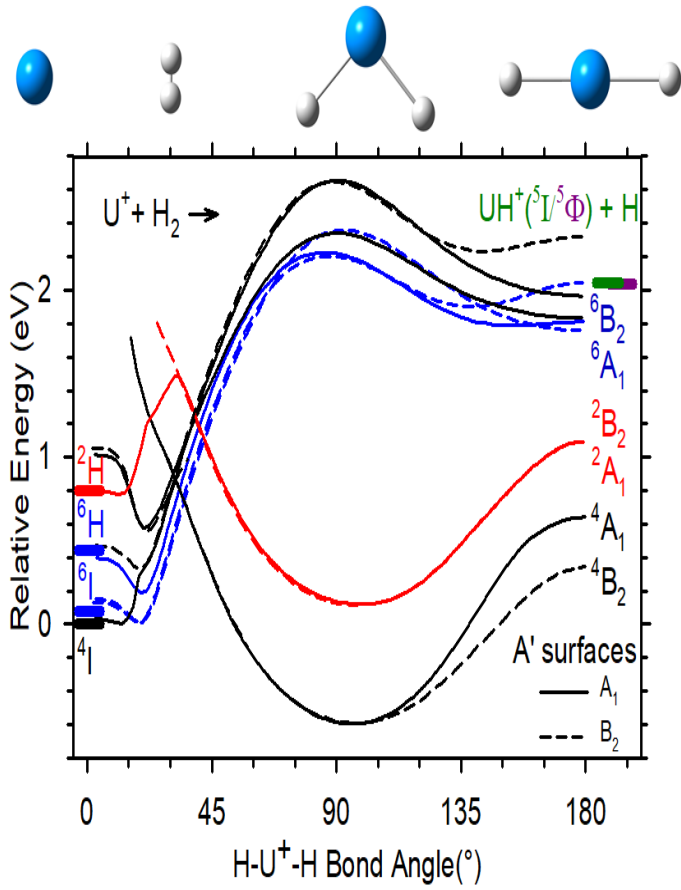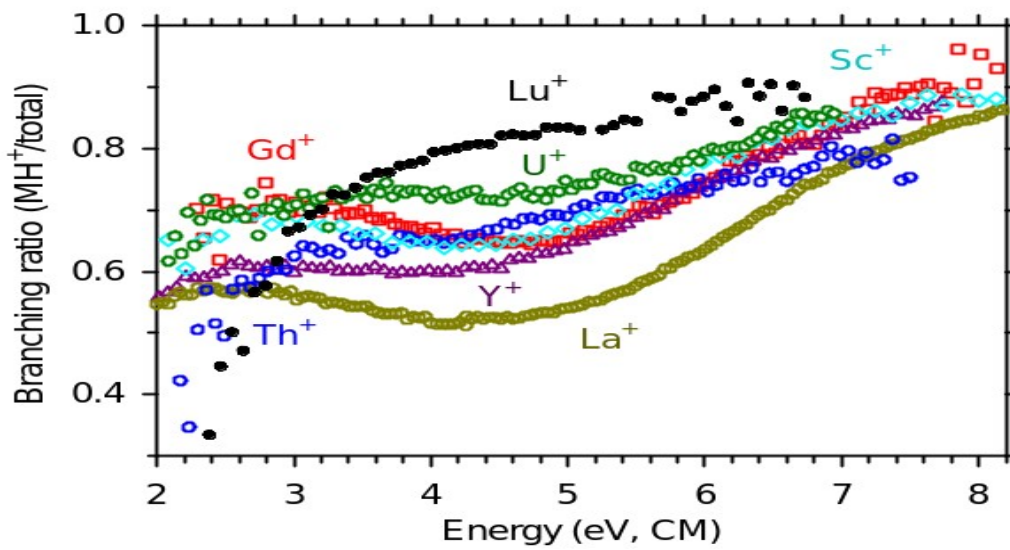
Figure 1

Figure 2

Figure 3

Figure

Figure

TOC graphic

U⁺ + H₂ ⟶
UH⁺ + H

$D_0(U^+-H) =$
2.48 ± 0.06 eV

U⁺ + HD ⟶
UH⁺ + D
UD⁺ + H
Cross Section
Energy (eV)